Analysis of a Folded Plate Sandwich Panel Roof System Using Assumed Stress Hybrid Elements

Krishnan Gowri

A Thesis

in

The Centre for Building Studies

Presented in Partial Fulfillment of the Requirements
for the degree of Master of Engineering at
Concordia University
Montréal, Québec, Canada

April 1984

© Krishnan Gowri, 1984

ABSTRACT

Analysis of a Folded Plate Sandwich Panel Roof System Using Assumed Stress Hybrid Elements

Krishnan Gowri

In single storey commercial and industrial buildings, the roof can be integrated with passive solar glazings to achieve energy savings in space heating and daytime illumination. The geometry of a folded plate sandwich panel roof can be chosen to provide an appropriate angle for the glazings, thereby increasing the seasonal efficiency in solar energy collection. Sandwich panels with good structural resistance properties, can satisfy the required insulation standards. The structural analysis of such a roofing system is complicated because of the unusual geometry, composite materials and the openings used for glazings. The available structural analysis procedures are reviewed and the assumed stress hybrid finite element technique is found to be suitable for analyzing the proposed roofing system. Rectangular stress hybrid bending elements are formulated using simple assumed stress functions and their convergence properties are investigated. The bending elements are combined with membrane elements to generate ten different shell elements. A special purpose finite element program has been developed for the analysis. A prismatic folded plate has been analyzed using these elements and the results are compared with experimental values. An

analytical roof model has been chosen and a stress analysis is performed to study the load deformation characteristics of the proposed structural system. A series of parametric analyses is carried out to study the effect of certain material properties on the structural behaviour of the roof system and the results are presented.

ACKNOWLEDGEMENT

I wish to express my gratitude and appreciation to Dr. P.P. Fazio for initiating this research and for his valuable guidance, criticisms and suggestions throughout this study.

I am thankful to Dr. H.K. Ha and Dr. M. Shapiro for their helpful suggestions and interest in this study.

The financial support of La Formation de chercheurs et d'Action Concertée du Québec (Equipe: Fazio et al) and National Science Research Council of Canada (Grant No. A-4770) is very much appreciated.

I extend my thanks to Prof. Rm. Sethunarayanan, Dr. S. Chockalingam, Dr. A.S. Rao and Dr. V.S. Alagars' family for their encouragement and interest in my education.

Additional thanks are due to Behdad, Luong, Martin, Parvaneh, Angie, Connie, Diane, Gisele, Nancy and all others at CBS for their help during the course of this study.

My special thanks to Mrs. Gloria Miller for her excellent and fast typing of this thesis.

With respect, love and admiration, I sincerely thank my parents and relatives for their encouragement and moral support.

And finally, to Vasanthi for her patience and affection.

TABLE OF CONTENTS

LIST OF FIGURES

LIST OF TABLES

NOTATIONS

a,b	dimensions of the element
$\beta_1,\beta_2, \ldots$	independent parameters
d	distance between centroids of facings
E	elastic modulus of facing material
G	shear modulus of core material
h	core thickness
M_x, M_y, M_{xy}	moment per unit length
ν	poission's ratio of facing material
Q_x, Q_y	shear force per unit length
θ_x, θ_y	rotations about x and y axis respectively
t	thickness of facings
u,v,w	displacements in x, y and z directions
U	strain energy in the plate element
$[k], [k_m], [k_b], [k_z]$	stiffness matrices
$[I], [H], [R], [N], [L]$	matrices used in formulating the stiffness matrix
$\{Q\}$	vector of nodal forces
$\{q\}$	generalized nodal displacement vector

CHAPTER I

INTRODUCTION

1.1 General

It is possible to enhance the economics of solar space heating by integrating the components of the solar collectors with that of the building thereby reducing the duplication of material and construction time.

In principle, there are two methods (11) in use for the collection of solar energy in space heating:

a. Flat plate collectors and

b. Building and its elements as collectors.

Flat plate collectors belong to the active solar energy system in which the collected energy is transported and delivered by mechanical means. The use of building and its components as collectors belong to the category of passive solar systems, in which the collection and utilization of solar energy is achieved by natural means of conduction, convection and radiation. In the building industry, solar architecture principles have been developed for the residential buildings of North America. Passive solar components are integrated with the structure to provide an economic and energy efficient building. For the integrated design of single storey commercial and industrial buildings, there is not much work reported. Because of the varying utilization of the enclosed space, it is very difficult to develop a general design procedure for such buildings. Of the total energy consumption, a typical

North American single storey commercial building consumes 48% for space heating, 24% for lighting, 12% for cooling and 12% for water heating (22). Hence the use of solar energy for space heating and daytime illumination can reduce substantially the amount of electrical load in commercial buildings. Since the problem of storage is not critical, it is possible to develop an industrialized integrated roofing system for this type of building.

1.2 Literature Review

Before the development of passive solar concepts, active solar collectors mounted on the roof of buildings were widely used for solar energy saving. One of the first few modern commercial buildings using solar energy is the La Quinta Motor Inns Inc., (5). The solar collection system has 19 flat plate collector panels covering 400 sq. ft. and 2500 gallon storage tank. This system operates in connection with conventional water to air heat pumps. The solar collectors are oriented on the roof and additional structural components have been used to keep the collector arrays in the appropriate position. Another example is the Carey Arboretum Science Building, New York (32). This is a two storey building with 27,400 sq. ft. of floor area. 85% of its space is solar heated by 5650 sq. ft. of two different water type collectors. The roof of the building is of saw-tooth form. There are six complete "teeth", 25 feet apart on centres, covering six bays. Each bay has several sky lights. Between successive teeth are 4 foot wide

horizontal walkways. All the skylights are made of double glazings and equipped with a shutter consisting of a rotating insulating vane, which can be operated manually. The solar collection is assisted by the white -- shingled reverse slopes of the "teeth". These slopes at 30 degrees from the horizontal, reflect additional solar radiation to the collectors. Many more case studies can be found in Ref. 32. Most of the earlier commercial buildings using solar energy are equipped with active systems.

A research report on solar flat plate collectors integrated with the roof, was done by J.D. Balcomb et al. (2) in 1975. The most important advantage has been the potential for cost and material savings due to combined functions. The integration of active solar components paved the way to the development of passive solar architecture. Active components have been found to be uneconomical because of the transportation loss and maintenance cost. Hence passive solar concepts gained importance in the planning and design of buildings. Most of the passive solar residential buildings have been constructed with a large area of south facing glazings. Skylights, also termed as roof apertures are used in the warmer regions to reduce the daytime electric load used in illumination. Lawrence Berkeley Laboratory has prepared reports about using roof apertures for office buildings in Atlanta, Los Angeles and in New York (29).

1.3 Scope and Objectives

The primary objective of this study is to develop a tool for the structural analysis of a sandwich panel roofing system which can integrate the passive solar glazings and to investigate the structural behaviour of such a system.

Among the available roofing systems, folded plates offer the possibility to integrate the passive glazing arrays at an appropriate angle. Folded plate roofs can span great distances with little material and with relatively simple formwork. A structurally efficient folded plate geometry can be chosen to integrate passive solar glazings which will have a good seasonal efficiency for space heating. Light weight three layer sandwich panels with good thermal resistant properties can be chosen as the roofing material. These kind of panels are suitable for simple fabrication, transportation and installation techniques.

The structural analysis of such a roofing system is complicated because of the unusual geometry of the roof and because of the composite behaviour of the materials used. The available structural analysis procedures have been reviewed and the numerical finite element technique based on hybrid stress formulation is used. Rectangular elements with simple assumed stress functions have been formulated and their suitability has been verified based on convergence tests. The use of finite element technique avoids several assumptions used by most of the existing folded plate theories. Also any arbitrary folded plate geometry of a roof can be analyzed. There is no restriction on the boundary

conditions and loading. An analytical roof model has been chosen to study the structural behaviour of the proposed roofing system. Effect of certain material properties on the maximum deflection of the roof system is also investigated.

1.4 Organization of the Thesis

Chapter II deals with the various factors involved in the selection of roof geometry and materials. It also includes a brief description of the proposed system and its limitations.

In Chapter III, the available structural analysis procedures relating to the folded plate theory and sandwich panels are reviewed. Their viability to solve the problem at hand is discussed.

Chapter IV describes the investigation carried out on the development of simpler rectangular stress hybrid elements. Various stress functions are used in formulating finite elements for bending and membrane actions. A convergence study is carried out on two numerical test cases. Ten different combination of shell-elements are generated for the analysis. The suitability of the shell elements are tested on a folded plate problem for which experimental test results are available.

Chapter V briefly explains the analytical roof model chosen for the analysis. It includes the description of the finite element idealization and the results of analysis. Effect of various material properties on the structural behaviour of the system are also investigated.

CHAPTER II

SELECTION OF ROOFING SYSTEM

2.1 Introduction

In single storey commercial and industrial buildings, passive glazings can be integrated either with the wall or the roof of a structure for solar energy saving. If the building encloses a large floor area and if it is provided with only south facing glazings oriented on the wall, then the solar radiation absorbed may not be sufficient to supply the required amount of energy for the interior. By placing the south facing glazings on the roof, the north section of the building can be solar heated directly. Also a uniform illumination of the working area can be achieved. The results of the study by Wayne Place et al (29) indicate that a large fraction of the electricity consumed for the daylighting in a single storey commercial building can be replaced by glazings integrated with the roof. This chapter deals with the various factors involved in the orientation of glazings, selection of roofing material and the description of the proposed system.

2.2 Collector Tilt Angle and Orientation

Passive systems use solar radiation that enters through the glazings directly into the space to be heated. Most of the solar radiation entering the building is converted to heat. Solar intensity on the glazings should be maximized to minimize the required area of glazings,

thereby minimizing both the capital cost of the glazing and the deleterious thermal effects of conductive gains and losses through the building envelope. The collection of solar radiation during the winter should be comparatively higher than the collection during summer, so that excess solar gains tend to occur more often during the heating season than during the cooling season. The sunlight entering the building through the glazings should provide uniform illumination of the working surface. Also there should be no problems of glare.

For good seasonal efficiency, the solar rays should be approximately normal to the glazing surface. The orientation of the glazings depend on the latitude of the site, economic considerations, architectural and user requirements of the building. For maximum year round collection, the south facing glazings should be tilted toward the equator at an angle slightly greater than the latitude of the site, by approximately five degrees. For summer collection, the best angle is latitude minus 10 to 15 degrees and for winter collection, latitude plus 10 to 15 degrees (25). The steeper the collector tilt angle, the lesser will be the problems of snow accumulation and rain. The orientation of the collector should favour the wind scouring of snow from the trough.

Collector array spacing should be chosen to avoid mutual shading of one array on to another. A general rule for collector spacing is that the shadow line of one collector array should intersect the bottom of the next collector array during the last two weeks of December (17). It is uneconomical to design the collector spacing for maximum saving on

December 21st, since the sun spends only a few days in that position near the winter solistice. Structural and economic considerations show that some shading has to be tolerated in order to achieve a sufficient ratio of collector to floor area.

As an example, for winter space heating in the Montreal region, assuming south facing glazings, the collector tilt angle can be calculated as shown below:

collector tilt angle = latitude + 10 to 15 degrees

= 45.5 + 15 = 60.5 ≈ 60 degrees.

When the altitude of the sun is less than 30 degrees, all the glazing arrays excepting the first one will be shaded and the shaded glazings can absorb only reflected and/or scattered radiation. Optimizing the fold geometry to receive maximum direct solar radiation during this period will result in increasing the tilt angle or the width of the horizontal separators. In either case, the structure becomes uneconomical and structurally inefficient.

2.3 Insulation and Storage

Proper insulation of the building envelope and the glazings are required to minimize the heat loss. The walls of the building should have a higher R value to meet the required insulation standards. (R value here refers to the insulating ability of the material). Anderson (1) suggests an R value of 40 for the buildings in colder climates.

Maximum heat is lost through the glazings when there is no solar gain. Therefore, the glazings have to be well insulated with shutters or with special type of venetian blinds to avoid the loss of thermal energy. A reflective insulating blind can be placed over the innerside of the glazings. This will avoid the excessive illumination and heating on certain area. Also the glare can be well controlled.

Since solar energy is not constantly available, some sort of storage is needed to sustain a solar powered thermal system through the nights and at times when the supply of solar energy is cut off by local weather conditions. The storage system has to be as close as possible, to the space where the energy has to be delivered. This is desirable to avoid the transportation loss from storage to the space requiring energy. Of the ones available, the phase change storage technique is found to be suitable for use in industrial systems (25). The phase change storage material can absorb great quantities of heat when they change from solid to liquid state. The same amount of heat is liberated when the material solidifies. The phase change material is light in weight and occupies less volume.

2.4 Selection of Roofing Material

The following is a list of suitable materials available for the proposed roofing system:

1. Concrete (reinforced, prestressed and lightweight)
2. Cold formed steel sheeting
3. Three layered sandwich panel

Concrete is a satisfactory material considering the thermal and structural characteristics. But the dead weight is much greater than the expected maximum live load of the roof. This makes the choice of concrete very uneconomical for single storey long span buildings. Light weight concrete is thermally efficient but the structural performance is not satisfactory for long span roofing and so it is not considered in this study (33).

Cold formed steel has a satisfactory load carrying capacity and is light in weight. But it has poor insulation characteristics and hence this material is not suitable for the proposed roofing system.

Sandwich panels can be factory fabricated and are ten to fifteen times lighter when compared to the traditional roofing material of equivalent strength. The core of the sandwich panel can be chosen to serve as an effective insulating material and it also adds to the transverse shear stiffness of the panel. The face material can be chosen to serve as vapour barriers and they add to the membrane stiffness of the panels. Since the panels are light in weight, no massive supporting structure is required for this type of roofing. Hence the sandwich panels are chosen to be the roofing material for the proposed system.

2.5 Description of the System

Fig. 2.1 shows a typical fold geometry suitable for winter space heating in the Montreal region. The passive solar glazings are inclined at 60° to the horizontal and the roofing panels are at 30° to the horizontal. Maximum reflected radiation will be directed toward the glazings, because the roofing panels are nearly at 90 degrees to the glazings. The glazings have to be provided with metallic extrusions. This metallic frame will rest on adjacent sandwich plates. The horizontal walkways will provide access to the glazing panels.

Double glazings made of fiber glass are proposed. These kind of glazings have a higher R value than the conventional glazings. Reflective insulating blinds (31) may be used to ensure the effective insulation of glazings.

For storage, the latent heat storage material usually packed in plastic coated foil pouches may be used. These bags of suitable size can be chosen and placed on the inner face of the roofing panels. The choice of storage is at the discretion of solar scientists.

A back up heating system, (ex. base board electric heaters) is necessary to supplement the solar thermal power system. View glazings on the side walls are suggested to satisfy the required lighting standards. These side wall glazings will reduce the glare on the working plane and will provide energy during December.

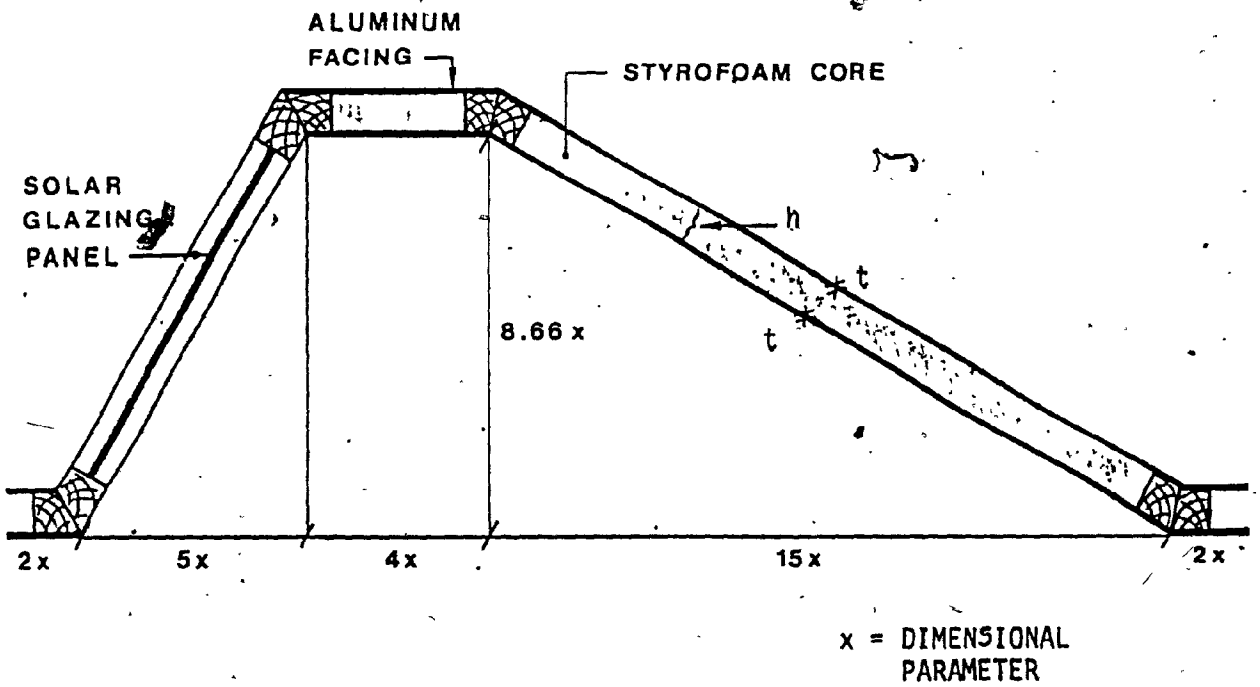

FIG. 2.1 TYPICAL FOLD GEOMETRY

A computer graphics routine has been developed using MEGATEK to delineate the roofing system. A typical view of a roof with six arrays of glazings is shown in Fig. 2.2.

2.6 Limitations of the System

The proposed system is suitable for single storey commercial buildings only. It is preferable and advantageous for long span structures. 100% of energy saving or space heating is not assured. This is true with all the solar powered systems in use. The roof sandwich panels have to be designed to safely resist the maximum accumulation of snow in the fold sections. The detailing and construction of the fold line joints are very important.

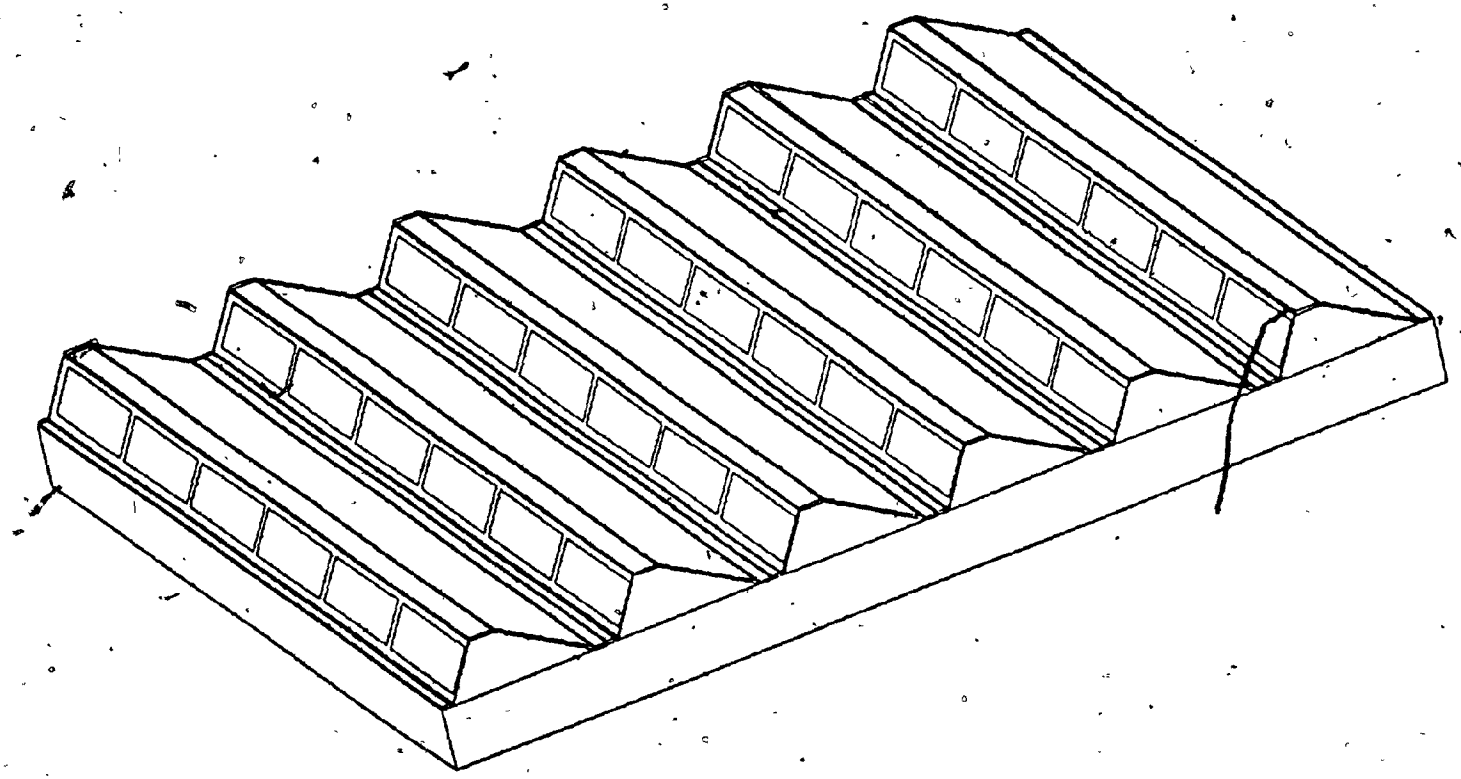

FIG. 2.2 TYPICAL VIEW OF ROOFING SYSTEM WITH SIX ARRAYS OF GLAZINGS

CHAPTER III

REVIEW OF AVAILABLE STRUCTURAL ANALYSIS PROCEDURES

3.1 Introduction

The proposed roofing system has an unusual and unsymmetrical folded plate geometry and is made up of composite materials. There is no closed form solution available for the analysis of such a structure. This chapter reviews the available methods of structural analysis related to the folded plates and sandwich panels, and their viability to solve the problem at hand is assessed.

3.2 Classification of Available Structural Analysis Procedures

Many authors have developed solution procedures for the analysis of folded plates and sandwich panels depending on a specific need. The available methods of structural analysis can be classified into the following four categories (based on assumptions and structural idealizations used):

i) Slab - beam method

ii) Classical folded plate theory

iii) Direct stiffness method and

iv) Approximate - numerical method.

3.3 Slab-Beam Method

A.H. Nilson (24) has used the slab-beam theory by separating the folded plate deformation into two different behaviours. In the transverse direction between fold lines, loads are carried by slab action and the loads applied to the surface being carried between fold lines by the bending strength of the surface. In the longitudinal direction, the reaction of all such transverse beam strips is applied as a line loading along the fold lines. The action of folded plate units in resisting this load is similar to that of inclined deep girders, laterally braced by adjacent plates, and spanning between the end walls of the structure. Fig. 3.1 shows the slab-beam action in a simple folded plate. The fold line joints are treated as hinges and hence there is no moment transfer between the plates. This theory has been used to analyze a light gauge steel folded plate and the results are shown to be in good agreement with that of an experimental testing of a prototype model.

A.G. Vinckier and M. Van Laethem of Belgium (33) analyzed a plywood folded sandwich plate roof by idealizing it to be of a statically determinate arch. A cross section of the roof and the idealization are shown in Fig. 3.2 and Fig. 3.3 respectively. Based on static equations of equilibrium, the in plane force in the plate is calculated and the thickness of facings are designed to resist this in plane force. The slab behaviour of the plates are not considered in this method. The results of the analysis using this method are reported to be within 5% of the experimental test results.

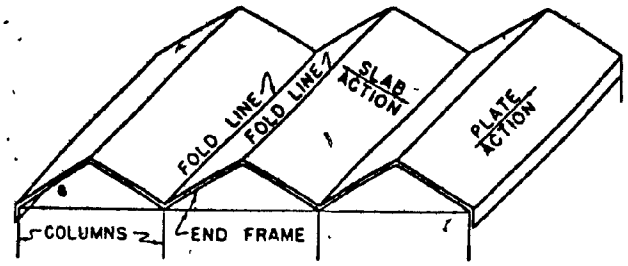

FIG. 3.1 SLAB BEAM ACTION (REF. 24)

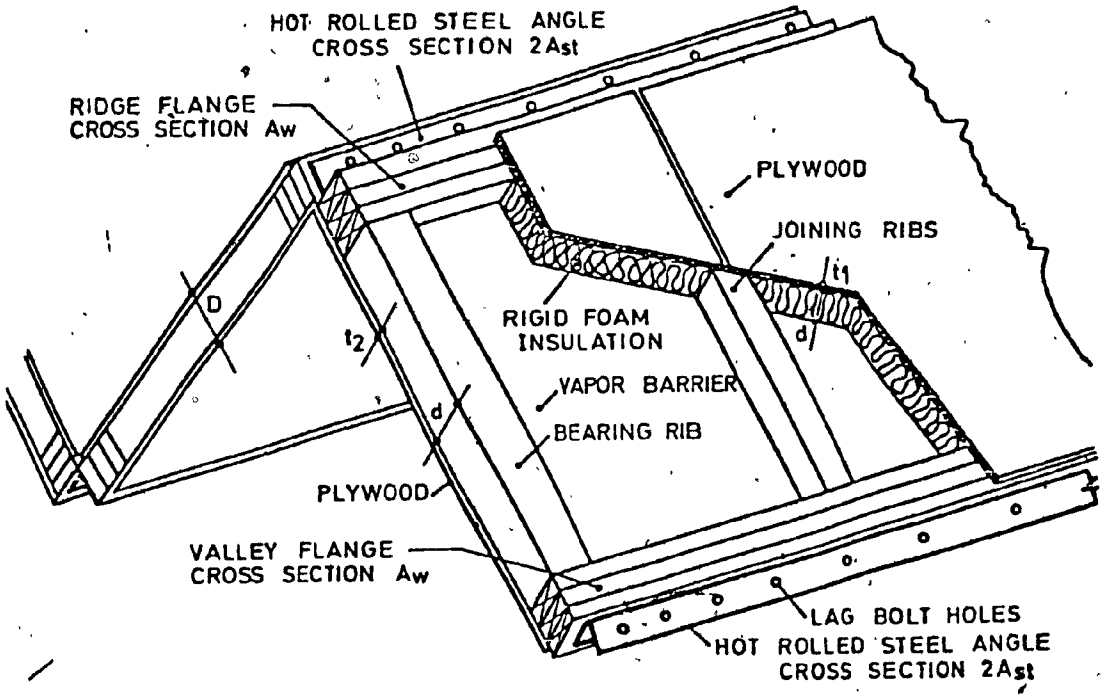

FIG. 3.2 CROSS-SECTIONAL VIEW OF FOLDED PLATE (REF. 32)

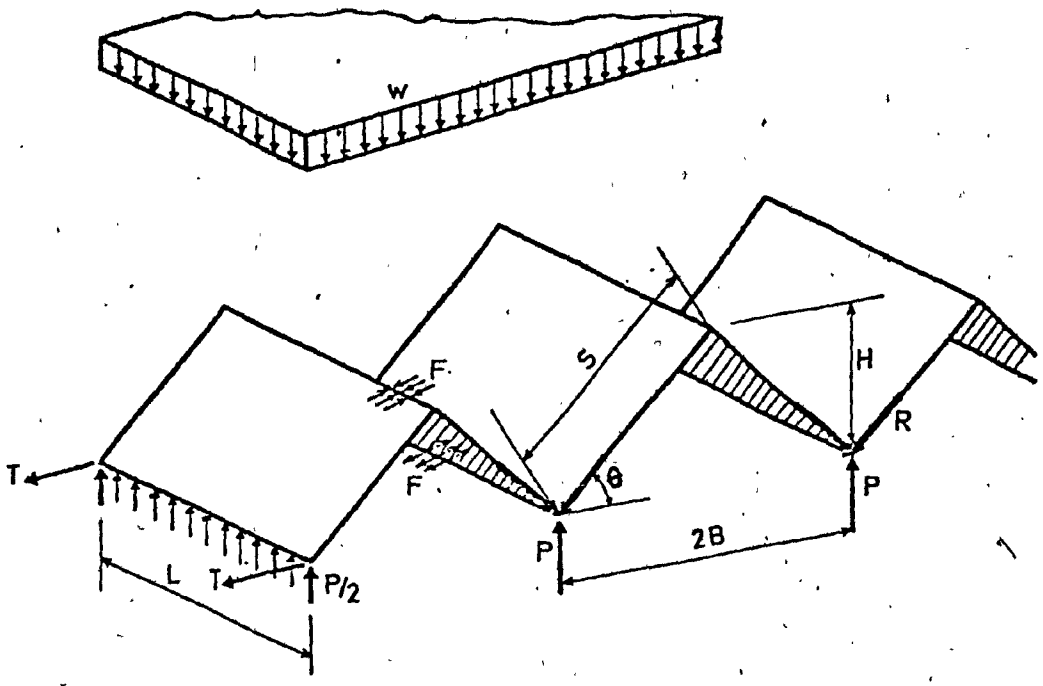

$$P = W\ B\ L$$

$$T = \frac{W\ B\ L}{4 \tan \theta}$$

$$R = \frac{W\ B\ L}{2 \sin \theta}$$

FIG. 3.3 IDEALIZATION OF THE SANDWICH PANEL FOLDED PLATE (REF. 32)

Both the above methods use a gross approximation. They are applicable only for prismatic folded plates of very long span. In such idealizations, it is not possible to take into account the transverse shear deformation of core in the sandwich plates. Also the application of this method is restricted to folded plates made of homogeneous materials.

3.4 Classical Folded Plate Theory

J.E. Goldberg and H.L. Leve (18) have developed an elasticity solution for the analysis of prismatic folded plates. The theory takes into consideration the simultaneous bending and membrane actions of the plates and yields a solution involving tabulated functions. The forces at the longitudinal edges of each slab are expressed as fixed edge forces modified by the effect of displacement of joints. The generalized displacements are taken to be four at each joint:

- two components of translation and a rotation (all lying in a plane, normal to that of the joint) and
- a translation in the direction of the joint.

Corresponding to these displacements, four force components have been considered at each longitudinal edge of the slab:

- a force in the plane of slab normal to its edge
- a shear in the direction of thickness
- a longitudinal shear and
- an edge moment.

The joint displacements are expanded in terms of a half range Fourier series. An arbitrary harmonic of one of the displacements is applied to one edge of the slab and the resulting homogeneous boundary value problem is solved for the displacements within the slab. These displacements define the resulting forces in the interior of the slab and they establish the forces at edge due to the displacement at one edge. The edge-displacement relation has been used to establish the joint equilibrium equations, as well as in evaluating the fixed edge forces of the loaded slabs. A general analysis procedure has been presented in Ref. 18.

The effect of transverse shear deformation in the plates has not been included in the analysis. This theory is suitable for folded plates made of homogeneous materials and the solution procedure is very long, tedious and cumbersome.

3.5 Direct Stiffness Methods

A. De Fries-Skene and A.C. Scordelis (10) used the ordinary theory of folded plates and formulated a stiffness matrix for each plate. The assembled stiffness matrix of the plate structure has been used in solving for the unknown displacements. Four independent displacement degrees of freedom are considered. In this method, the effect of shear deformation in the plates has not been taken into account.

P. Fazio and J.B. Kennedy (12) analyzed folded sandwich plate structures by extending the direct stiffness method described by

De Fries-Skene and Scordelis. Starting with the slope deflection equation and accounting for the transverse shear deformation of the core, an eight by eight stiffness matrix has been formulated for each plate. The stiffness for membrane and bending actions are calculated separately and using the principle of superposition, the element stiffness matrix is assembled. The element stiffness matrices are transformed to a global reference axis system and the structure stiffness matrix for the plate assembly is formed. Standard direct stiffness solution procedures are used in evaluating the displacements and stress resultants at each joint.

P. Fazio and J.F. Dewall (13) and G.M. Folie (16) independently modified Goldberg and Leve's theory for the analysis of sandwich folded plates and used the direct stiffness matrix formulation for the analysis.

All the methods described above are applicable only for prismatic folded plates. Composite folded plates with openings or with intermediate edge beams can not be analyzed.

3.6 Approximate - Numerical Methods

For a more general and practical application, the approximate numerical methods can be conveniently used. The analysis procedure consists of dividing the structure into elements, computing the stiffness of elements, assembling them into a structure stiffness matrix for the entire system, and solving that matrix for any applied load. The stress

resultants and displacements at any point on the structure can be evaluated. The major advantage of using such a technique is that there is no restriction on the material properties of the elements and also there is no restriction on the boundary conditions. The structural behaviour of a roof with openings and beam/bar members can be easily simulated by using this method. The available approximate numerical methods can be classified as:

i) Finite Element Method
ii) Finite Strip Method
iii) Finite Panel Method and
iv) Finite Layer Method

The finite strip method, finite panel method and the finite layer method can be viewed as special elements formulated using the finite element technique. The application of these elements is limited and is not dealt with in this study.

A number of finite elements have been developed for the analysis of folded plates and for sandwich plate bending. The available finite elements can be classified based on the formulation of the stiffness matrix:

i) Compatible models
ii) Equilibrium models
iii) Mixed models and
iv) Hybrid models.

In formulating the stiffness matrix by compatible model, the displacement functions are chosen to satisfy complete compatibility

along interelement boundaries. In such a formulation, the stress equilibrium is not satisfied within each element. Whereas in the equilibrium model, stress functions are chosen to satisfy equilibrium conditions, which result in the violation of interelement compatibility requirement. In general, the solutions obtained by using compatible models are lower bound and that of equilibrium models are upper bound.

In mixed models, neither displacements nor stresses are given preferential treatment. Also, a mixed model may require more degrees of freedom than a displacement model to achieve a given accuracy. Generally, mixed models can predict stresses more closely than the assumed displacement formulation (9).

Hybrid elements can be of various types. The most successful is the assumed stress hybrid, in which compatible displacement functions are assumed along the interelement boundaries, in addition to the equilibrating stress field in each element. The solutions using hybrid elements are much closer to the exact and may be either upper bound or lower bound or even oscillating about the exact. A comparison of all the finite element formulations are reported by T.H.H. Pian and P.Tong (27).

Rockey and Evans applied the displacement element for the analysis of folded plates. This element does not consider the effect of transverse shear deformation of the plate and is applicable only for homogeneous folded plates. A refined higher order displacement element for folded plate analysis is reported by J.E. Beavers and F.W. Beaufit (4).

This element has too many degrees of freedom and is also not applicable for non homogeneous plates.

A number of finite elements are available for the analysis of sandwich plates in bending. A detailed study on the available sandwich elements is done by B. Jafari-Naini (23). Assumed stress hybrid models are identified to be suitable for developing bending elements which account for transverse shear deformation.

The important feature of hybrid elements is that the transverse shear deformation of the sandwich core is taken into account without introducing any additional degrees of freedom other than the displacements and edge rotations, and the derivation of the stiffness matrix is simpler. A shell element of six degrees of freedom per node can be formulated to analyze sandwich panel folded plates. The required compatibility criterion can be satisfied by assuming a suitable displacement function along the element boundaries. Hence the assumed hybrid stress elements are used in analyzing the proposed roofing system.

CHAPTER IV

FORMULATION OF SIMPLER RECTANGULAR HYBRID ELEMENTS

4.1 Introduction

For sandwich plate analysis, two rectangular hybrid stress elements are available at present (3,16). Both these elements assume a linear variation in edge displacements along the boundaries and a complete quadratic stress distribution over the domain of the element. The derivation of the stiffness matrix for these elements is very long and involves tedious matrix operations, because of the assumed quadratic stress distribution. Also the results obtained using such elements are expected to be conservative for predicting deflections, because of the seventeen independent parameters used in the assumed stress function. A.J. Barnard (3) has assumed that the thickness of facings are much less than the thickness of core and hence for a larger thickness of facings, the results obtained using this element will be much more flexible than that of Fazio and Ha (15). Three triangular elements with linear stress modes have been reported by R.D. Cook (6,7). To form a general quadrilateral/rectangular element, four such triangular elements have to be used and the degrees of freedom associated with the central node have to be statically condensed to that of the corner nodes. This chapter deals with the investigation carried out in formulating simpler rectangular hybrid stress elements for the analysis of sandwich folded plate structures. The stiffness matrices for bending and membrane actions are derived independently and assembled to form a general six degrees of

freedom per node shell element. Ten shell element combinations are generated from five bending elements and two membrane elements. The suitability of these elements are tested on a folded plate problem whose experimental results are available.

4.2 Assumptions

The following are the assumptions used in the stiffness matrix formulation of the rectangular sandwich plate elements:

1. Displacements and strains are small and the materials obey Hooke's law.
2. Perfect bonding exists between the faces and the core of the sandwich, so that no slip can occur.
3. Transverse displacements across a section normal to the middle surface are the same.
4. Bending stiffness of the facings about their own plane and the shear stresses in the facings are neglected.
5. The core resists only transverse shear stresses. Normal stresses in directions parallel to the faces are neglected and
6. Local buckling of the faces due to membrane stresses is not considered.

4.3 Formulation of Bending Elements

Consider a rectangular sandwich plate of dimensions a, b consisting of a core thickness 'h' and facings of equal thickness 't' (fig. 4.1). The facings and the core of the sandwich panel to be treated here are of isotropic material. (Orthotropic materials and unequal thickness of facings can be analyzed with minor modifications).

The strain energy in the element due to bending action is (21),

$$U = \tfrac{1}{2} \int_0^b \int_0^a \left[\frac{2}{Etd^2}\left[M_x^2+M_y^2-2\,\nu\,M_x\,M_y+2(1+\nu)M_{xy}^2\right] + \frac{1}{Gh}\left[Q_x^2+Q_y^2\right]\right]dx\,dy$$

where $d = h + t$

Fig. 4.2 shows a rectangular sandwich element which has three degrees of freedom at each node: rotations θ_x and θ_y and transverse deflection w. The stiffness matrix for this element has been derived using the assumed stress hybrid technique. The summarized procedure from Ref. 20 is given in Appendix A. The approach is simple and well documented in Ref. 27 and hence will not be discussed in detail here.

Four different assumed stress modes using five, seven, nine and eleven independent β parameters are used. The assumed stress distributions used in each case is given below:

(i) Five stress mode (RH5B):

$$M_x = \beta_1 + \beta_4\,\bar{x}$$

$$M_y = \beta_2 + \beta_5\,\bar{y}$$

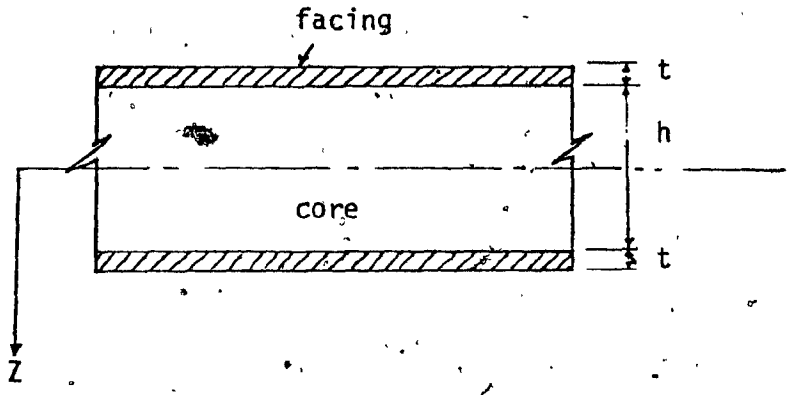

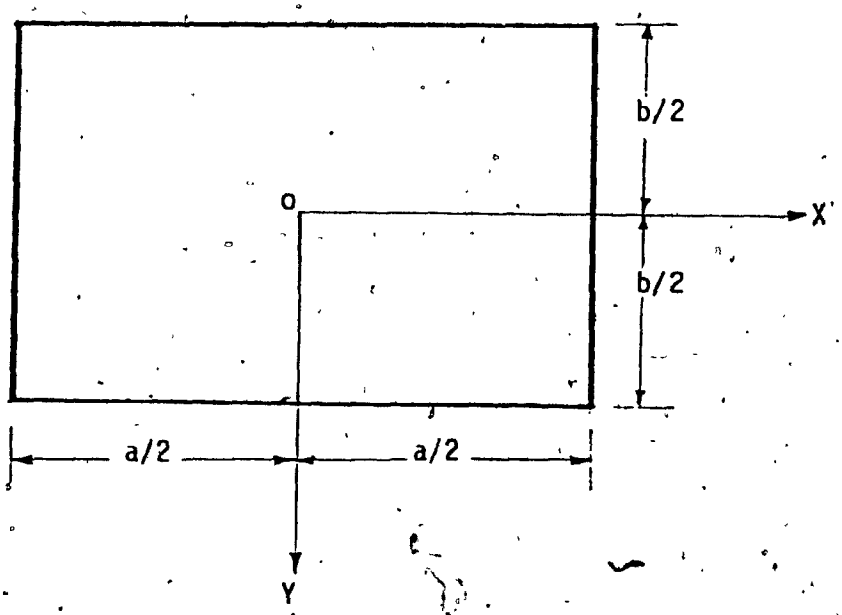

FIG. 4.1 CROSS SECTIONAL VIEW AND GEOMETRY OF THE SANDWICH PLATE

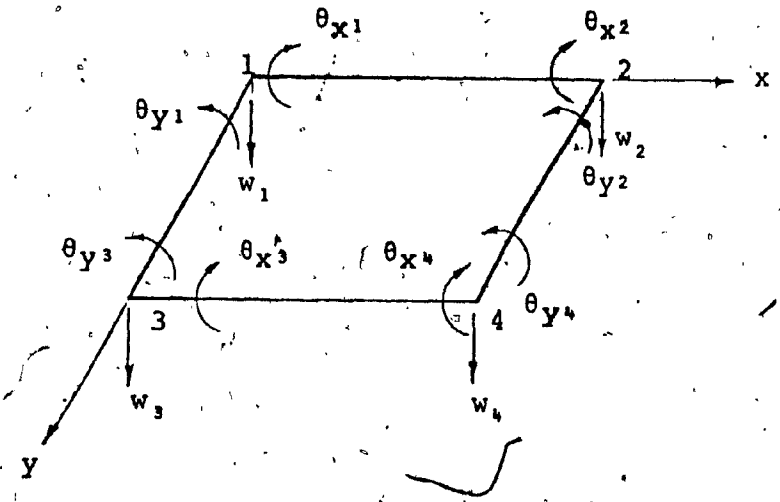

FIG. 4.2: NODAL DISPLACEMENTS FOR BENDING ACTION

$$M_{xy} = \beta_3$$

$$Q_x = \beta_4/a$$

$$Q_y = \beta_5/b$$

(ii) Seven stress mode (RH7B):

$$M_x = \beta_1 + \beta_4 \bar{x} + \beta_6 \bar{y}$$

$$M_y = \beta_2 + \beta_5 \bar{y} + \beta_7 \bar{x}$$

$$M_{xy} = \beta_3$$

$$Q_x = \beta_4/a$$

$$Q_y = \beta_5/b$$

(iii) Nine stress mode (RH9B):

$$M_x = \beta_1 + \beta_4 \bar{x} + \beta_7 \bar{y}$$

$$M_y = \beta_2 + \beta_5 \bar{x} + \beta_8 \bar{y}$$

$$M_{xy} = \beta_3 + \beta_6 \bar{x} + \beta_9 \bar{y}$$

$$Q_x = \beta_4/a + \beta_9/b$$

$$Q_y = \beta_6/a + \beta_8/b$$

(iv) Eleven stress mode (RH11B):

$$M_x = \beta_1 + \beta_4 \bar{x} + \beta_7 \bar{y} + \beta_{10} \bar{x}\bar{y}$$

$$M_y = \beta_2 + \beta_5 \bar{x} + \beta_8 \bar{y} + \beta_{11} \bar{x}\bar{y}$$

$$M_{xy} = \beta_3 + \beta_6 \bar{x} + \beta_9 \bar{y}$$

$$Q_x = \beta_4/a + \beta_9/b + \beta_{10} \bar{y}/a$$

$$Q_y = \beta_6/a + \beta_8/b + \beta_{11} \bar{x}/b$$

The complete quadratic stress mode (RH17B) used by Ha (20) has the following stress distribution:

$$M_x = \beta_1 + \beta_2 \bar{x} + \beta_3 \bar{y} + \beta_4 \bar{x}^2 + \beta_5 \bar{x}\bar{y} + \beta_6 \bar{y}^2$$

$$M_y = \beta_7 + \beta_8 \bar{x} + \beta_9 \bar{y} + \beta_{10} \bar{x}^2 + \beta_{11} \bar{x}\bar{y} + \beta_{12} \bar{y}^2$$

$$M_{xy} = -\left(\frac{b}{a} \beta_4 + \frac{a}{b} \beta_{12}\right) \bar{x}\bar{y} + \beta_{13} + \beta_{14} \bar{x} + \beta_{15} \bar{y} + \beta_{16} \bar{x}^2 + \beta_{17} \bar{y}^2$$

$$Q_x = \frac{\beta_2}{a} + \frac{\beta_4}{a} \bar{x} + \frac{\beta_5}{a} \bar{y} - \frac{a}{b^2} \beta_{12} \bar{x} + \frac{\beta_{15}}{b} + \frac{2}{b} \beta_{17} \bar{y}$$

$$Q_y = -\frac{b}{a^2} \beta_4 \bar{y} + \frac{\beta_9}{b} + \frac{\beta_{11}}{b} \bar{x} + \frac{\beta_{12}}{b} \bar{y} + \frac{\beta_{14}}{a} + \frac{2}{a} \beta_{16} \bar{x}$$

in which $\bar{x} = x/a$, $\bar{y} = y/b$ and β are the unknown stress parameters.

The above assumed stress distributions satisfy the following homogenous equations of equilibrium of a differential element (fig. 4.3) subjected to bending action:

$$\frac{\partial M_x}{\partial x} + \frac{\partial M_{xy}}{\partial y} - Q_x = 0$$

$$\frac{\partial M_y}{\partial y} + \frac{\partial M_{xy}}{\partial x} - Q_y = 0 \qquad \text{and}$$

$$\frac{\partial Q_x}{\partial x} + \frac{\partial Q_y}{\partial y} + q = 0$$

where q is the intensity of transverse loading.

For all the elements, a linear variation of the generalized edge displacements is assumed. For example along edge 1-2,

$$w_{1\_2} = w_1 (1-\bar{x}) + w_2 \bar{x}$$

$$\theta_{x_{1\_2}} = \theta_{x_1} (1-\bar{x}) + \theta_{x_2} \bar{x}$$

$$\theta_{y_{1\_2}} = \theta_{y_1} (1-\bar{x}) + \theta_{y_2} \bar{x}$$

The linear variation of edge displacements assures displacement continuity along the fold lines of a three dimensional folded plate structure. The admissibility of the above assumption is confirmed by Cook and Ladkany (8).

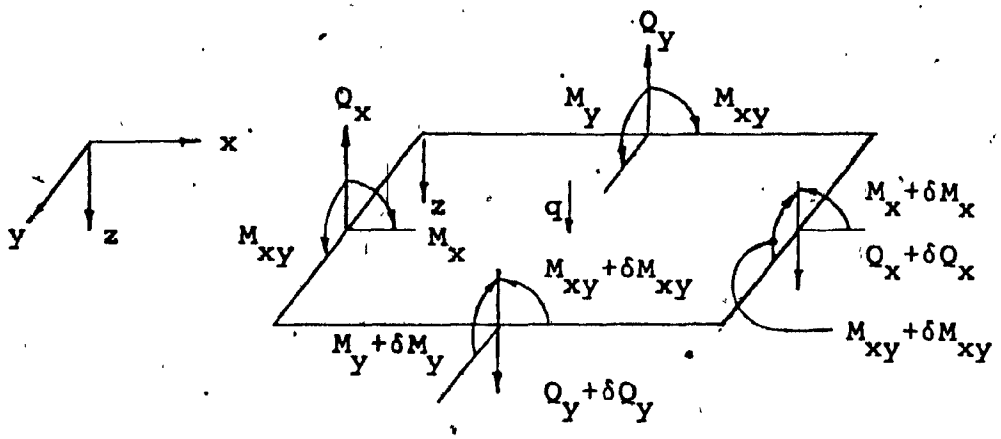

FIG. 4.3 EDGE FORCES ON A DIFFERENTIAL ELEMENT.

By means of complementary strain energy principle, the stiffness matrix of the element can be shown to be (26):

$$[K] = [T]^T [H]^{-1} [T]$$

where $[H] = \int_{vol} [P]^T [N] [P] \, dv$ and

$$[T] = \int_{S_i} [R]^T [L] \, ds$$

in which [P] represents assumed stresses

[N] contains material properties

[R] expresses surface force in terms of the undetermined β parameters and

[L] expresses the generalized edge displacements in terms of nodal displacements

S_i refers to the line integral along the element boundaries.

The explicit forms of [H] and [T] along with [P], [N], [R] and [L] for the RH11B element are given in Appendix B. FORTRAN subroutines for stiffness matrix generation of all the above elements are listed in Ref. 19.

4.4 Convergence Test

Two numerical test cases are analyzed using the four elements described earlier. The results are compared with the RH17B element and with analytical solutions. The sandwich plate problems considered here are a simply supported square plate and a clamped square plate, subjected to uniformly distributed transverse loading. The material properties and the geometry of the plates are shown in Fig. 4.4 and Fig. 4.5. Because of the symmetry in geometry and in loading, only a quarter of the plate needs to be analyzed. Various mesh sizes are considered in the analysis. The calculated central deflection and the maximum moment in each mesh size for all the five elements are given in Table 4.1 to Table 4.4. The ratio of computed value to the exact analytical solutions is plotted in Fig. 4.6 to Fig. 4.9.

(i) Convergence for Central Deflection:

It can be seen from Fig. 4.6 and Fig. 4.7 that the linear stress mode elements and the RH11B have a rapid convergence rate when compared with that of the RH17B element. The rate of convergence decreases with the increase in the number of independent β parameters used in the assumed stress function. As the mesh size is refined, the linear stress mode elements converge towards the exact, but the RH11B and RH17B elements stay asymptotic. When coarser meshes are used, RH17B element gives better results than that of the linear stress mode elements. It can be seen that the deflections predicted by the RH17B element and the RH11B element are almost the same.

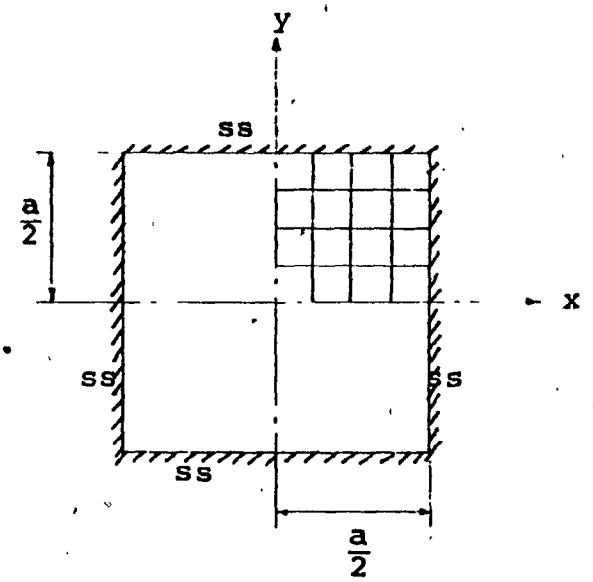

$q = 1\ lb/in^2$

$a = 120\ in$

$t = 0.025\ in$

$h = 1.975\ in$

$E = 10^7\ psi$

$G_c = 189\ psi$

FIG. 4.4 SIMPLY SUPPORTED SQUARE PLATE SUBJECTED TO UNIFORM LOAD

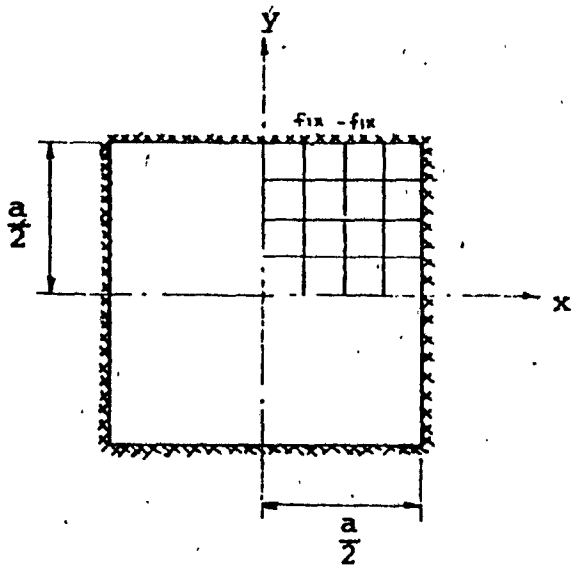

$q = 1\ lb/in^2$

$a = 120\ in$

$t = 0.025\ in$

$h = 1.975\ in$

$E = 10^7\ psi$

$\nu = 0.3$

$G_c = 744.\ psi$

FIG. 4.5 CLAMPED SQUARE PLATE SUBJECTED TO UNIFORM LOAD

NO.	MESH SIZE	RH5B	RH7B	RH9B	RH11B	RH17B
1	2 * 2	- 4.951	- 4.843	- 4.764	- 4.543	- 4.539
2	3 * 3	- 4.603	- 4.558	- 4.525	- 4.446	- 4.446
3	4 * 4	- 4.497	- 4.472	- 4.454	- 4.414	- 4.414
4	5 * 5	- 4.452	- 4.436	- 4.424	- 4.400	- 4.400
5	6 * 6	- 4.428	- 4.417	- 4.409	- 4.392	- 4.392
6	7 * 7	- 4.413	- 4.405	- 4.399	- 4.387	- 4.387
7	8 * 8	- 4.405	- 4.399	- 4.395	- 4.386	- 4.386
EXACT (analytical) (Ref. 30)		- 4.292				

TABLE 4.1

COMPUTED CENTRAL DEFLECTION (in inches) - SIMPLY SUPPORTED SQUARE PLATE.

NO.	MESH SIZE	RH5B	RH7B	RH9B	RH11B	RH17B
1	2 * 2	- 1.488	- 1.439	- 1.385	- 1.313	- 1.280
2	3 * 3	- 1.338	- 1.315	- 1.292	- 1.268	- 1.250
3	4 * 4	- 1.290	- 1.277	- 1.264	- 1.252	- 1.244
4	5 * 5	- 1.269	- 1.260	- 1.252	- 1.245	- 1.239
5	6 * 6	- 1.257	- 1.252	- 1.246	- 1.241	- 1.237
6	7 * 7	- 1.250	- 1.246	- 1.242	- 1.238	- 1.236
7	8 * 8	- 1.246	- 1.243	- 1.240	- 1.237	- 1.235
EXACT (analytical) (Ref. 30)		- 1.225				

TABLE 4.2

COMPUTED CENTRAL DEFLECTION (in inches) - CLAMPED SQUARE PLATE

NO.	MESH SIZE	RH5B	RH7B	RH9B	RH11B	RH17B
1	2 * 2	-721.88	-801.11	-736.37	-747.15	-736.20
2	3 * 3	-704.64	-740.41	-711.41	-712.91	-711.31
3	4 * 4	-698.08	-718.09	-701.83	-702.28	-701.94
4	5 * 5	-695.02	-707.78	-697.39	-697.58	-697.53
5	6 * 6	-693.35	-702.20	-695.00	-695.09	-695.11
6	7 * 7	-692.27	-698.76	-693.47	-693.53	-693.56
7	8 * 8	-691.82	-696.79	-692.74	-692.77	-692.81
EXACT (analytical) (Ref. 30)		- 689.76				

TABLE 4.3

COMPUTED MAXIMUM STRESS (in psi) - SIMPLY SUPPORTED SQUARE PLATE

NO.	MESH SIZE	RH5B	RH7B	RH9B	RH11B	RH17B
1	2 * 2	613.25	614.24	489.41	543.95	511.94
2	3 * 3	637.53	647.74	546.96	563.41	553.97
3	4 * 4	644.47	651.31	569.72	577.09	573.08
4	5 * 5	645.81	650.96	582.89	586.83	584.82
5	6 * 6	646.04	649.87	591.58	593.94	592.80
6	7 * 7	645.62	648.61	597.71	599.25	598.55
7	8 * 8	645.39	647.75	602.58	603.64	603.19
EXACT (analytical) (Ref. 30)		590.4				

TABLE 4.4

COMPUTED MAXIMUM STRESS (in psi) - CLAMPED SQUARE PLATE

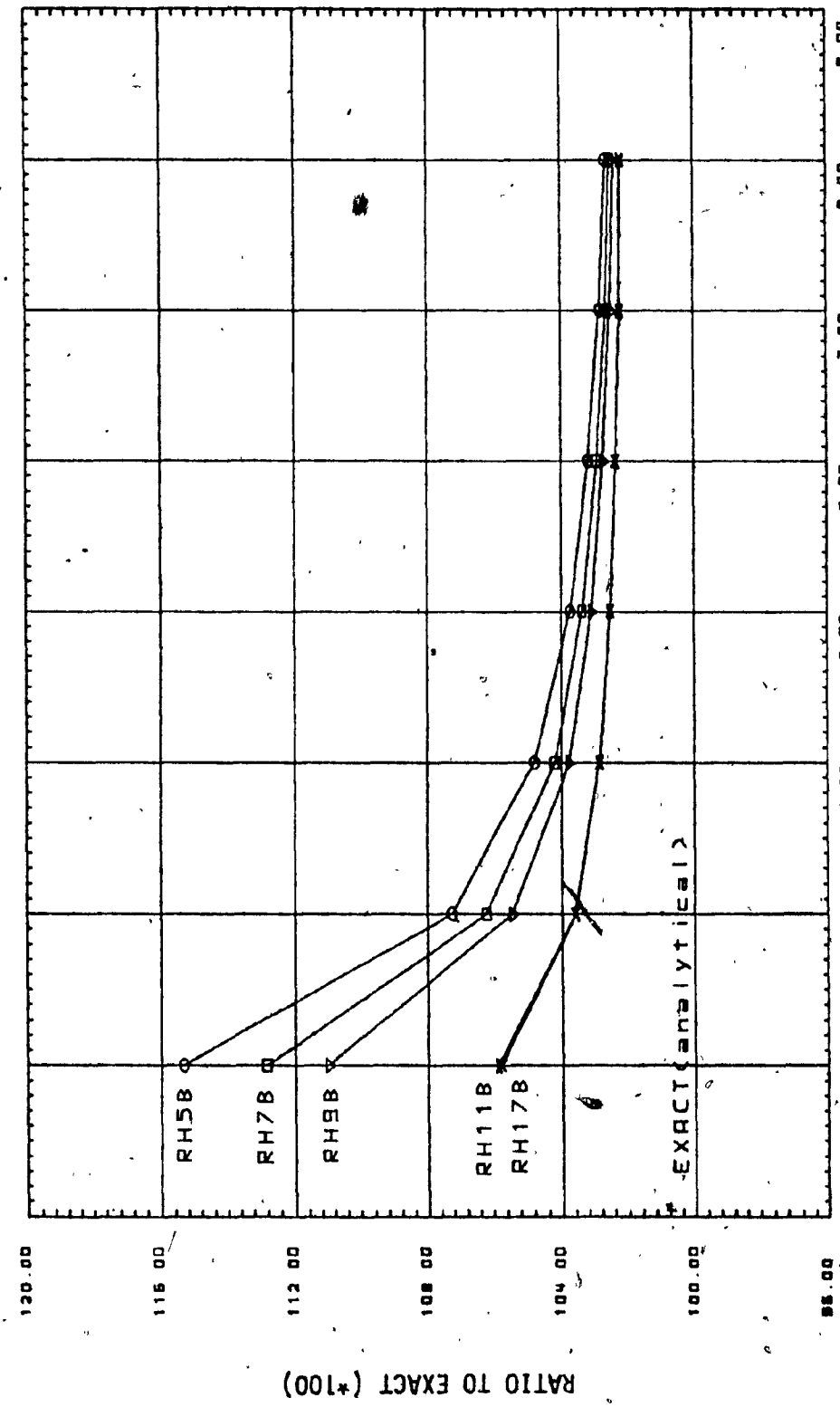

FIG. 4.6 CONVERGENCE OF MAXIMUM DEFLECTION
SIMPLY SUPPORTED SQUARE PLATE

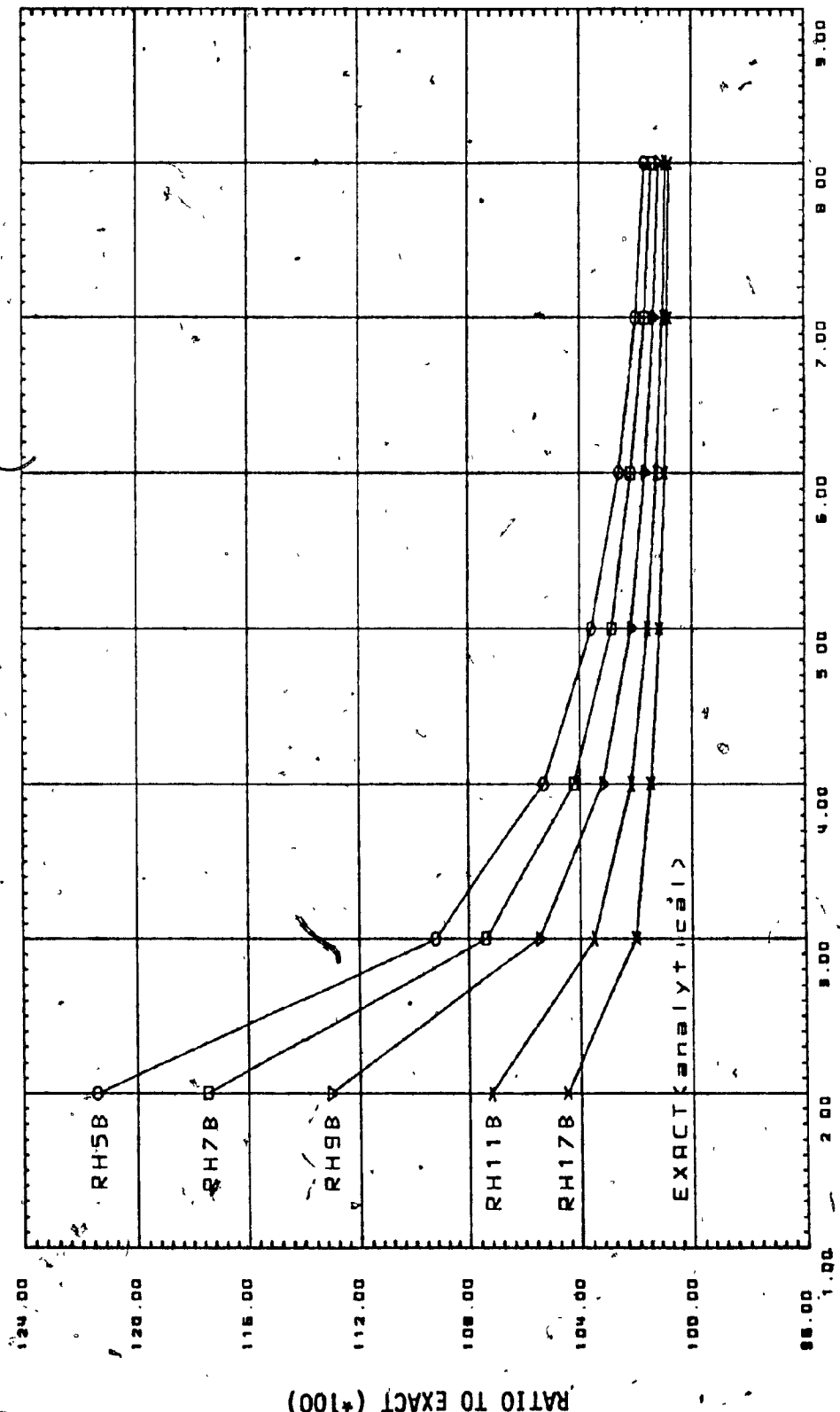

FIG. 4.7 CONVERGENCE OF MAXIMUM DELFECTION
CLAMPED SQUARE PLATE

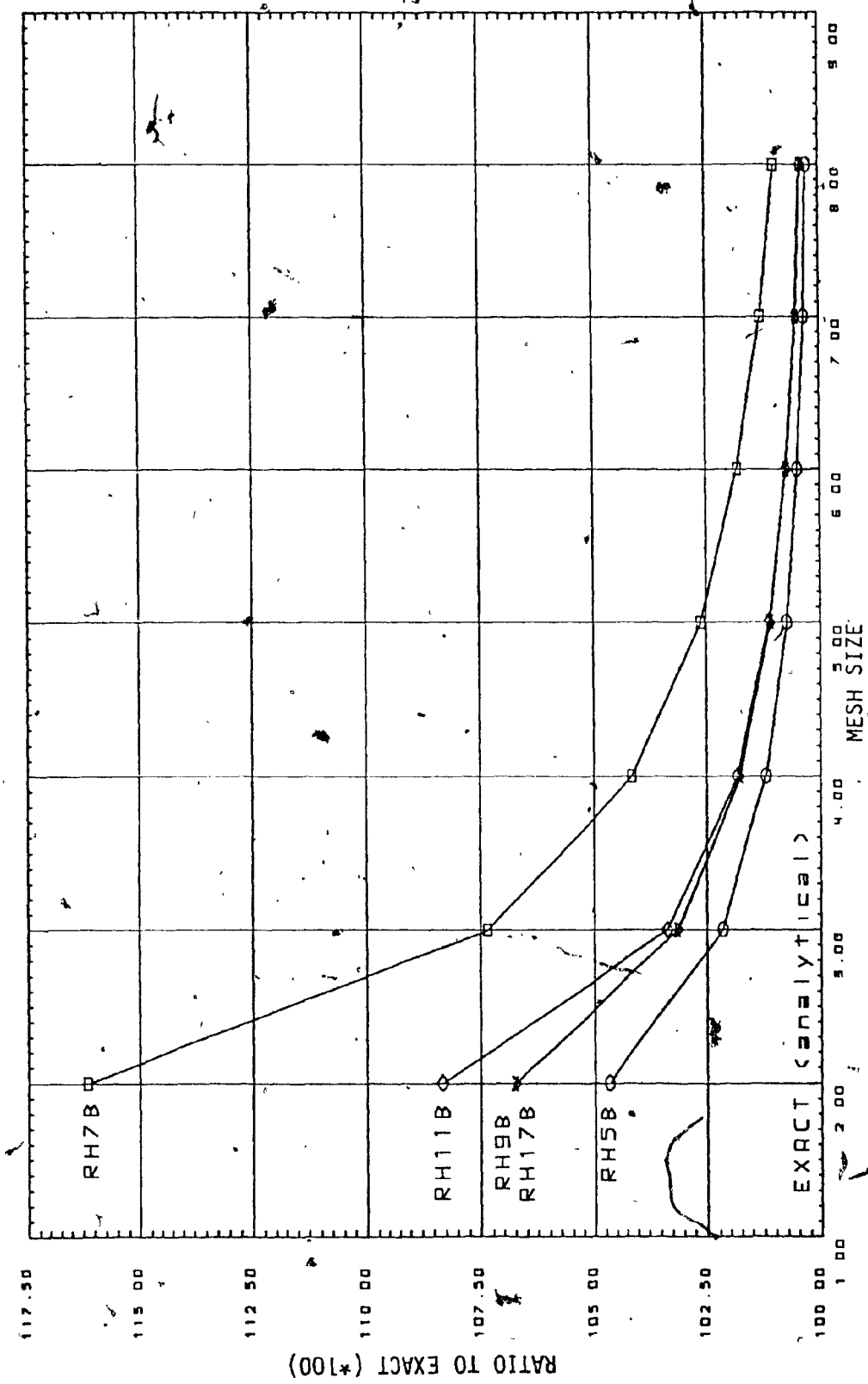

FIG. 4,8 CONVERGENCE OF MAXIMUM MOMENT
SIMPLY SUPPORTED SQUARE PLATE

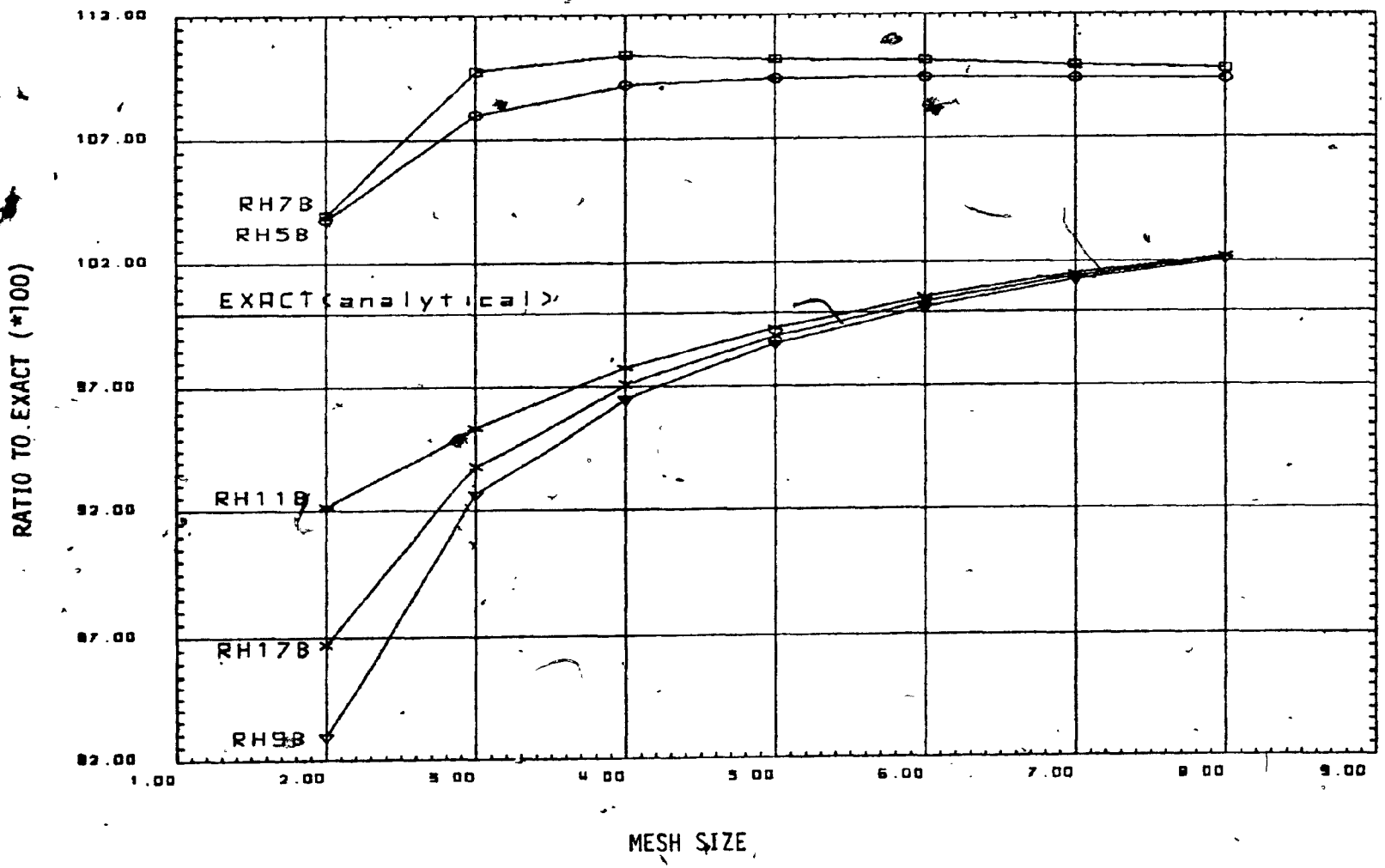

FIG. 4.9 CONVERGENCE OF MAXIMUM MOMENT
CLAMPED SQUARE PLATE

(ii) Convergence for Maximum Moment:

In the case of a clamped square plate, the maximum stresses evaluated using the RH5B and RH7B elements converge toward a wrong value. RH9B, RH11B and RH17B elements follow the same pattern and predict satisfactory values, closer to the exact solution even with a coarse mesh.

The RH9B element is found to be having two zero energy modes, in addition to the rigid body modes. In particular, for anticlastic plate bending problems, all the linear stress mode elements are found to be unsuitable, because of the missing $\overline{xy}$ term in the assumed stress function (28).

4.5 Formulation of Membrane Elements

Two rectangular membrane elements RH5M and RH7M having an assumed linear stress distribution with linear edge displacements are formulated using the stress hybrid technique. The nodal degrees of freedom are shown in Fig. 4.10. The assumed stress distribution for the elements are:

(i) Five stress mode (RH5M):

$$\sigma_x = \beta_1 + \beta_2 \bar{y}$$

$$\sigma_y = \beta_3 + \beta_4 \bar{x}$$

$$\tau_{xy} = \beta_5$$

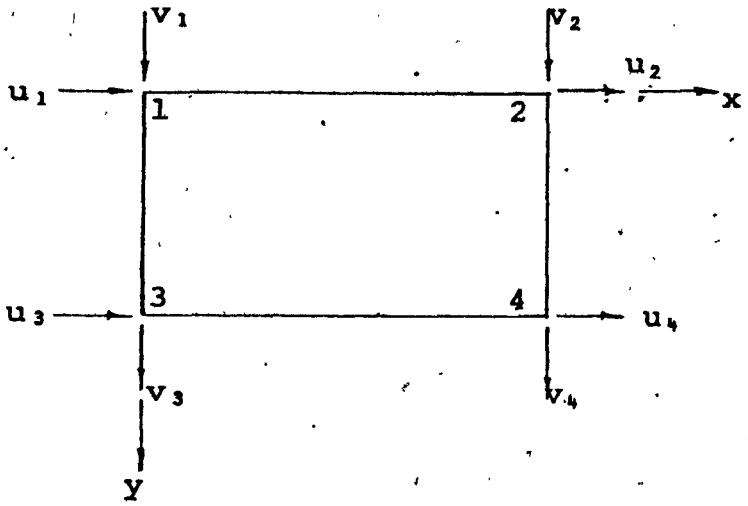

FIG. 4,10 NODAL DISPLACEMENTS FOR MEMBRANE ACTION

(ii) Seven stress mode (RH7M):

$$\sigma_x = \beta_1 + \beta_2 \bar{x} + \beta_3 \bar{y}$$

$$\sigma_y = \beta_4 + \beta_5 \bar{x} + \beta_6 \bar{y}$$

$$\tau_{xy} = \beta_7 - \frac{b}{a} \beta_2 \bar{y} - \frac{a}{b} \beta_6 \bar{x}$$

To ensure compatibility, linear edge displacements are assumed along the edges. For example along edge 1-2,

$$u_{1-2} = (1-\bar{x})\, u_1 + \bar{x}\, u_2$$

$$v_{1-2} = (1-\bar{x})\, v_1 + \bar{x}\, v_2$$

The stiffness matrix for these two elements are formulated in a manner similar to that of the bending elements. The details of matrix [P], [N], [R], [L], [T] and [H] for RH7M element are given in Appendix C.

The complete quadratic stress mode membrane element using twelve independent β parameters, used by Fazio and Ha (15) is found to give exactly the same results as the RH7M element.

4.6 Assembly of the Six Degrees of Freedom Per Node Shell Element

The membrane and bending actions of an element are characterized by the stiffness equations,

$$\{Q_m\} = [k_m]\ \{q_m\}$$

$$\{Q_b\} = [K_b]\ \{q_b\}$$

where the subscripts m and b refer to the membrane and bending actions respectively. By principle of superposition the stiffness matrix for the bending and membrane actions can be put in the form:

$$\begin{Bmatrix} Q_m \\ Q_b \end{Bmatrix} = \begin{bmatrix} k_m & 0 \\ 0 & k_b \end{bmatrix} \begin{Bmatrix} q_m \\ q_b \end{Bmatrix}$$

It should be noted that the in plane and bending actions are uncoupled within an element. This assumption is valid when the deformations of the element are small.

To facilitate the transformation of forces and displacements in three dimensional space and for general applications, it is necessary to include the fictitious in-plane rotational degrees of freedom. The corresponding force displacement relationship will be:

$$\{Q_z\} = [K_z]\ \{q_z\}$$

combining the above,

$$\begin{Bmatrix} Q_m \\ Q_b \\ Q_z \end{Bmatrix} = \begin{bmatrix} k_m & 0 & 0 \\ 0 & k_b & 0 \\ 0 & 0 & K_z \end{bmatrix} \begin{Bmatrix} q_m \\ q_b \\ q_z \end{Bmatrix}$$

Because q_z does not affect the strain energy in an element subjected to bending and membrane actions, the stiffness matrix $[k_z]$ should be a null matrix. However, to avoid the ill-conditioning of the stiffness matrix, small and arbitrary values are assigned to k_z. The details of matrix k_z are described in Ref. 20.

A FORTRAN IV program FEASP (19) has been developed to generate ten different stiffness matrices for shell elements. Any one of the five bending elements can be combined with RH7M or RH5M to form a shell element. All the ten shell elements are tested on a folded plate problem whose experimental results are available for comparison purposes. The description of the test problem and the results of the analysis are discussed in the next section.

4.7 Analysis of 19 Foot Folded Plate

Since the stresses in folded plates are caused by both membrane and bending actions, the complete stiffness matrix which includes both types of action must be used. Along the intersection of the panels which make up the folded plate, continuity of displacements and normal slopes should be maintained; these compatibility requirements are satisfied by the elements described earlier.

Fig. 4.11 shows the folded plate to be analyzed. It consists of six similar sandwich panels rigidly connected by means of aluminium channels, which were welded together at four inches interval. The panels were made up of 0.025 inch thick aluminium facings, bonded to an one inch thick honeycomb core. Details of the connections and the test procedures are fully reported in Ref. 12.

For the finite element analysis, rectangular elements and beam elements are used to idealize the panels and reinforcing channels respectively. A coarse mesh of six by ten (Fig. 4.12) is used in the analysis. The structure is subjected to a uniform pressure of 26 psf.

Table 4.5 to 4.8 show the calculated displacements and longitudinal stresses (in top facings) at the mid-span section of the folded plate, for each combination of the shell element. Since the membrane action is dominant in folded plates, combination of any one of the bending elements with a membrane element (either RH7M or RH5M) gives almost identical results. The RH5M element combination gives a more flexible solution when compared to that of RH7M. But it is interesting to note that the solutions obtained from RH5M combination agrees with that of the experimental deflection observed at the right extreme edge, whereas the solutions obtained using the RH7M combination of elements agree with that of the experimental deflection observed at the left extreme ridge. Good agreement between finite element solutions and experimental tests can be observed for stress resultants.

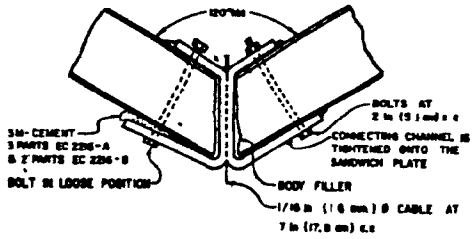

RIDGE CONNECTION DETAIL

FIG. 4.11 THE 19 FOOT FOLDED SANDWICH PLATE. ALUMINUM FACINGS, POLYSTYRENE CORE.

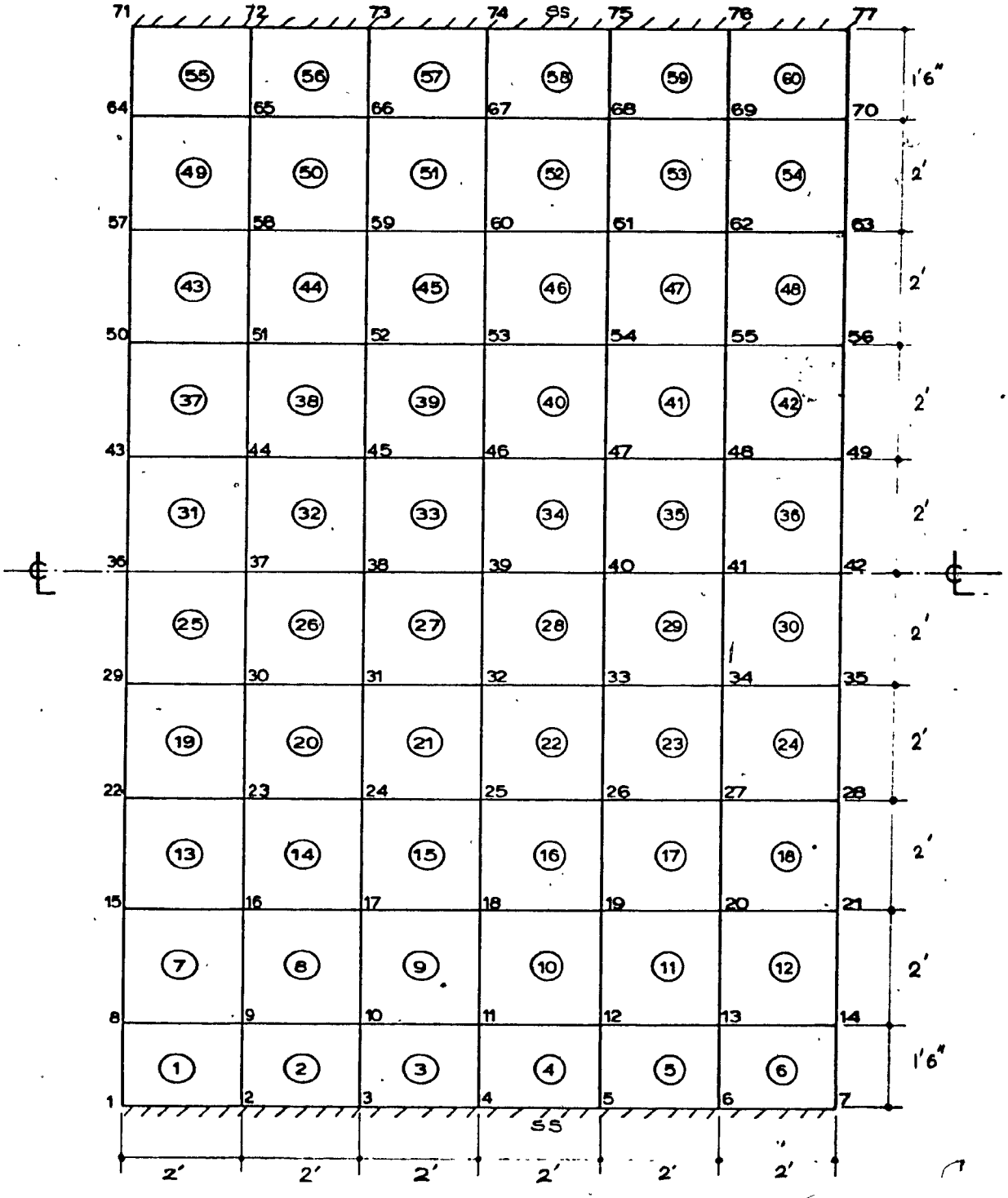

FIG. 4.12 FINITE ELEMENT MESH FOR THE 19 FOOT SANDWICH FOLDED PLATE.

ELEMENT COMBINATION	RIDGE 1	RIDGE 2	RIDGE 3	RIDGE 4	RIDGE 5	RIDGE 6	RIDGE 7
RH5B RH5M	- 0.987	- 0.575	- 0.571	- 0.546	- 0.571	-0.575	- 0.987
RH7B RH5M	- 0.984	- 0.575	- 0.571	- 0.545	- 0.571	- 0.575	- 0.984
RH9B RH5M	- 0.978	- 0.575	- 0.571	- 0.545	- 0.571	- 0.575	- 0.978
RH11B RH5M	- 0.976	- 0.575	- 0.571	- 0.545	- 0.571	- 0.575	- 0.976
RH17B RH5M	- 0.976	- 0.573	- 0.571	- 0.546	- 0.571	- 0.573	- 0.976
Experimental	- 0.940	- 0.491	- 0.504	- 0.371	- 0.500	- 0.572	- 0.995

TABLE 4.5

MID SPAN DEFLECTION (in inches) OF 19 FOOT FOLDED PLATE

ELEMENT COMBINATION	RIDGE 1	RIDGE 2	RIDGE 3	RIDGE 4	RIDGE 5	RIDGE 6	RIDGE 7
RH5B RH7M	- 0.957	- 0.542	- 0.538	- 0.513	- 0.538	- 0.542	- 0.957
RH7B RH7M	- 0.953	- 0.542	- 0.538	- 0.513	- 0.538	- 0.542	- 0.953
RH9B RH7M	- 0.948	- 0.542	- 0.538	- 0.512	- 0.538	- 0.542	- 0.948
RH11B RH7M	- 0.946	- 0.542	- 0.538	- 0.512	- 0.538	- 0.542	- 0.946
RH17B RH7M	- 0.946	- 0.540	- 0.538	- 0.513	- 0.538	- 0.540	- 0.946
Experimental	- 0.940	- 0.491	- 0.504	- 0.371	- 0.500	- 0.572	- 0.995

TABLE 4.6

MID SPAN DEFLECTION (in inches) OF 19 FOOT FOLDED PLATE

ELEMENT COMBINATION	RIDGE 1	RIDGE 2	RIDGE 3	RIDGE 4.	RIDGE 5	RIDGE 6	RIDGE 7
RH5B RH5M	- 5376.9	5765.93	- 6011.24	4746.06	- 6011.24	5765.93	- 5376.97
RH7B RH5M	- 5751.84	6054.50	- 6119.54	4743.90	- 6119.54	6054.54	- 5751.84
RH9B RH5M	- 5676.07	5984.91	- 6093.62	4736.91	- 6093.62	5984.91	- 5676.07
RH11B RH5M	- 5690.69	5986.04	- 6094.98	4736.48	- 6094.98	5986.04	- 5690.69
RH17B RH5M	- 5715.73	5889.11	- 6146.46	4721.23	- 6146.46	5889.11	- 5715.73
Experimental	- 5000	4000	- 5600	3500	- 5380	5650	- 4900

TABLE 4.7

LONGITUDINAL STRESSES (in psi) ALONG THE MIDSPAN SECTION OF 19 FOOT FOLDED PLATE

ELEMENT COMBINATION	RIDGE 1	RIDGE 2	RIDGE 3	RIDGE 4	RIDGE 5	RIDGE 6	RIDGE 7
RH5B RH7M	- 4682.55	5113.73	- 5308.5	4121.46	- 5308.5	5113.73	- 4682.55
RH7B RH7M	- 5057.47	5402.18	- 5416.53	4119.48	- 5416.53	5402.18	- 5057.47
RH9B RH7M	- 4981.10	5332.40	- 5396.03	4112.63	- 5396.03	5332.40	- 4981.10
RH11B RH7M	- 4995.57	5333.50	- 5392.47	4112.28	- 5392.47	5333.50	- 4995.57
RH17B RH7M	- 5023.45	5240.01	- 5442.86	4096.97	- 5442.86	5240.01	- 5023.45
Experimental	- 5000	4000	- 5600	3500	- 5380	5650	- 4900

TABLE 4.8

LONGITUDINAL STRESSES (in psi) ALONG THE MIDSPAN SECTION OF 19 FOOT FOLDED PLATE

From the results of test problems it can be concluded that the use of RH17B element can be avoided by replacing it with the RH11B element. The shell element formed by combining the RH11B and RH7M is seen to be performing well when compared to that of other combinations.

CHAPTER V

STRUCTURAL BEHAVIOUR OF ROOFING SYSTEM

5.1 Introduction

A three fold, 20 feet (6096 mm) span analytical roof model shown in Fig. 5.1 has been chosen to study the structural behaviour of the proposed system. The material properties of the sandwich panel used in the analysis correspond to that of a 19 feet span experimental, symmetric sandwich folded plate tested by Fazio (12,14). The roof structure is assumed to be simply supported on all the sides along the boundary. The roofing sandwich panels are connected along the fold lines using aluminum extrusions the connection details are given in Ref. 12. The size of the glazing panels used in the analysis are 30" x 15" (762 mm x 381 mm). These glazings are assumed to be framed with aluminum extrusions. The structural behaviour of the roofing system is simulated using rectangular assumed stress hybrid finite elements. The roof is subjected to a uniform pressure of 26 psf (1.245 K Pa). A series of analysis has been performed to study the change in maximum deflection due to the following:

i) Effect of shear modulus of core
ii) Effect of elastic modulus of facings
iii) Effect of thickness of core
iv) Effect of thickness of facings
v) Effect of span of roofing and
vi) Effect of number of folds.

Span of the roof: 20 ft.
TF - Thickness of Facings: 0.025 in.
TC - Thickness of core: 1.0 in.
E - Elastic Mod. of Faces: 10^7 psi
G - Shear Mod. of core: 260 psi

Edge Beam Properties:

Area of cross section 0.18 in^2
Moment of inertia 0.04 in^4
Polar moment of inertia 0.25 in^{-3} in^4

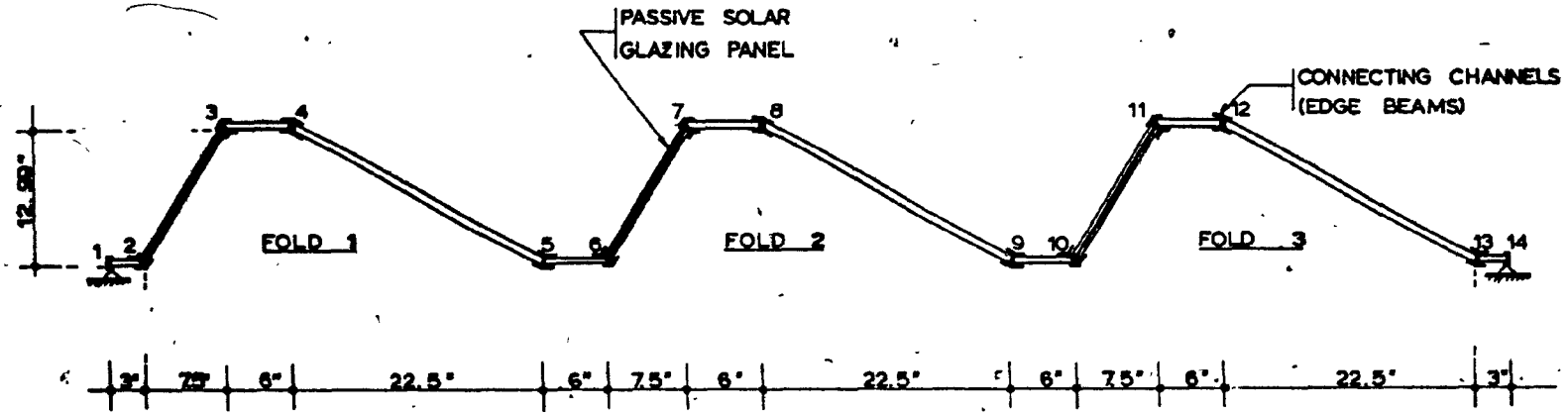

FIG. 5.1 CROSS SECTION OF THE ANALYTICAL ROOF MODEL

5.2 Description of Analysis

Taking the advantage of symmetry in geometry and loading, only one half the span of the roof model has been analyzed. Fig. 5.2 shows the finite element mesh used in the analysis. The discretized roof consists of 52 elements and 70 nodes. The width of each rectangular element equals the distance between the consecutive fold lines and the length equals to thirty inches. The fold line joints are represented by beam elements, the properties of which are input as edge beam for each element. The area of glazings have been treated as openings. An element type having the stiffness of the edge beams alone, has been used to replace the openings.

The program FEASP (19) has been used for the analysis. Six degrees of freedom per node shell elements formulated by combining the RH11B and RH7M elements are chosen for use in this analysis. Six sets of analyses have been done to study the effect of certain parameters on the structural performance of the roof system. In each set of analysis, only one parameter is varied while keeping all the others same. The details of the analysis and the results are discussed in the next section.

5.3 Results of Analysis

The deformed shape of the fold lines are shown in Fig. 5.3 to Fig. 5.5. From the graphs on fold line displacements, it can be noted that the fold lines bracing the solar glazings undergo almost the same pattern of displacement across the span. The in plane deformation of

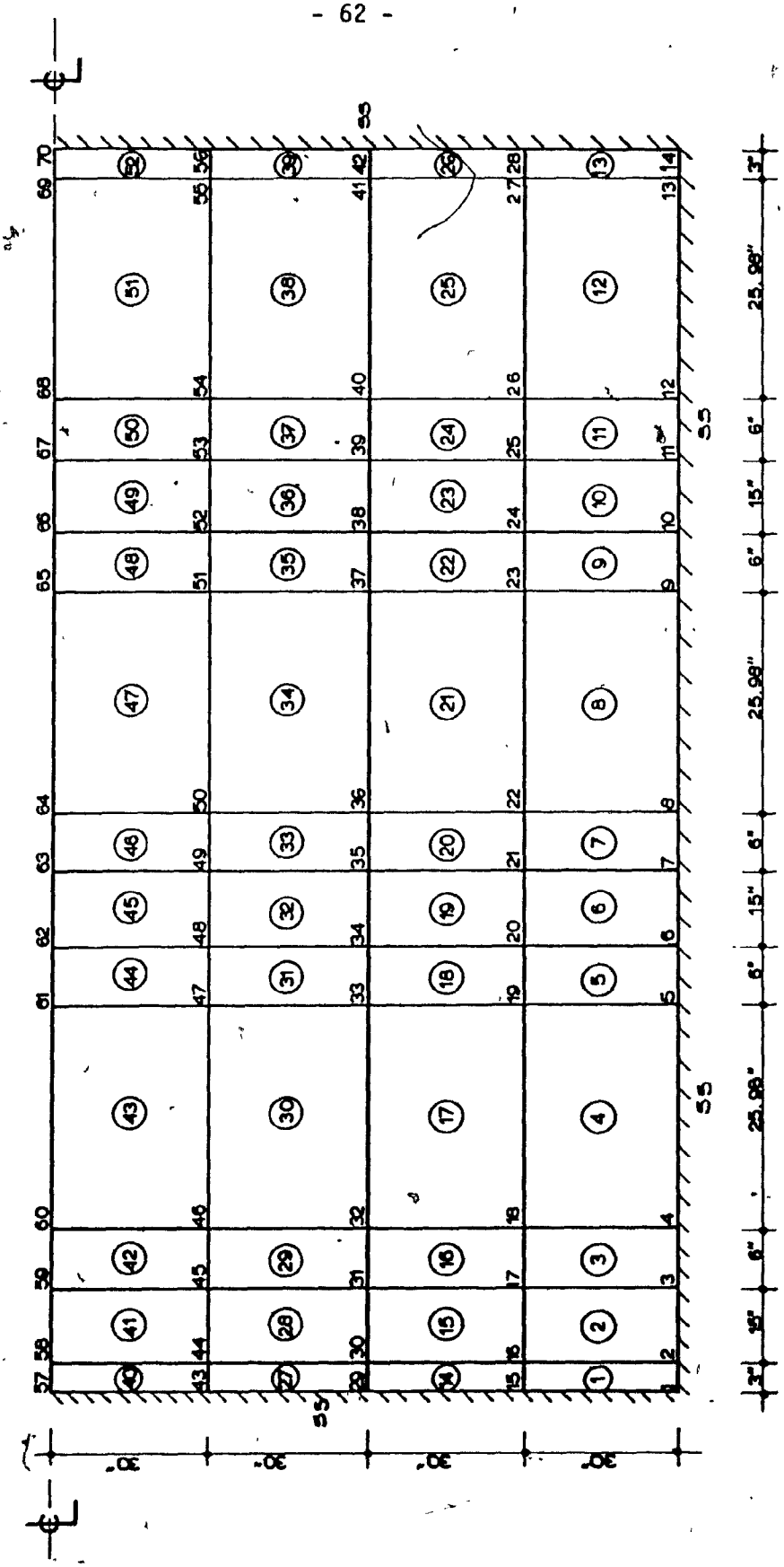

FIG. 5.2 FINITE ELEMENT MESH FOR THE IDEALIZED HALF SPAN

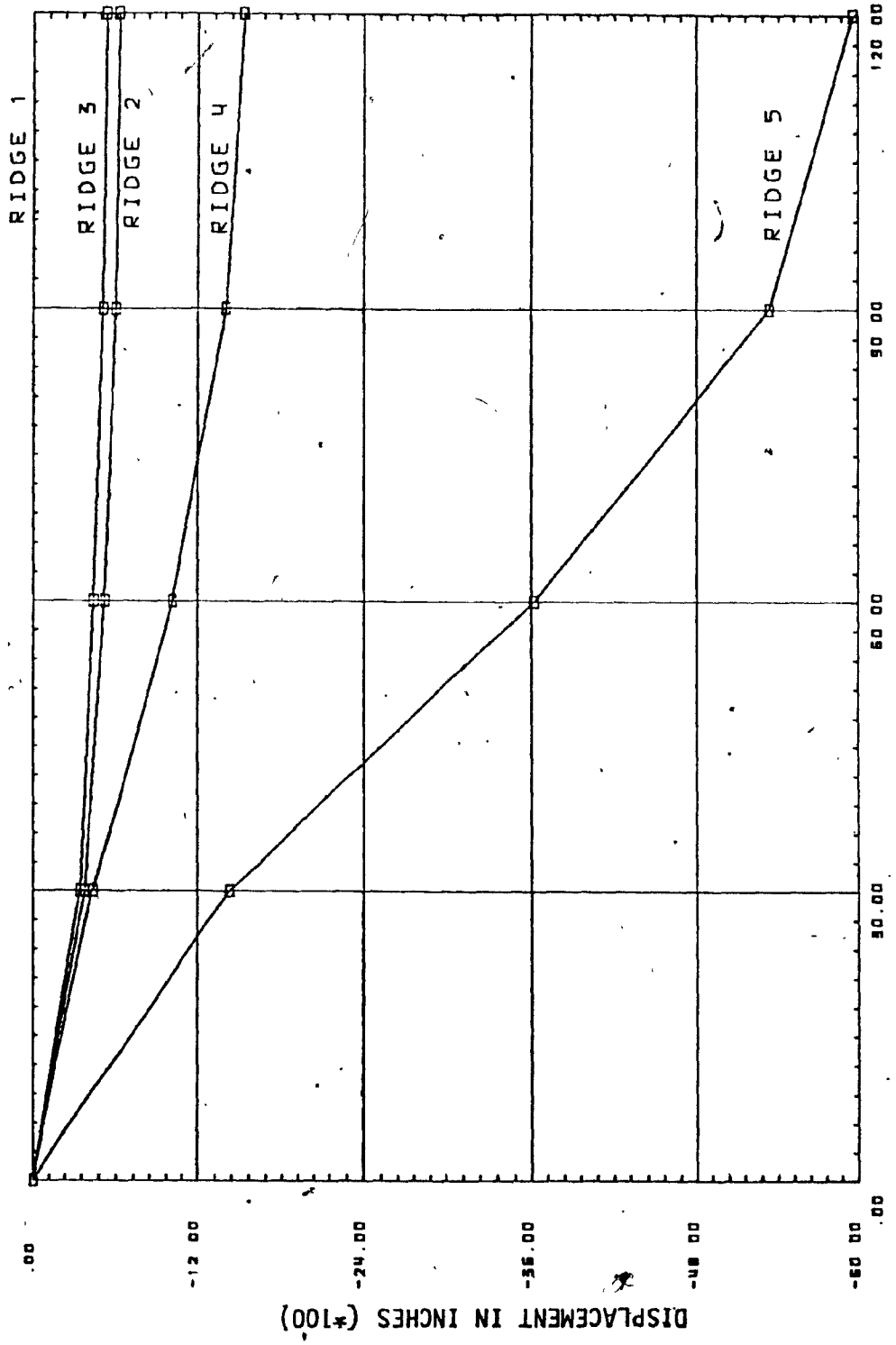

FIG. 5.3 FOLD LINE DEFORMED SHAPE OF FOLD 1

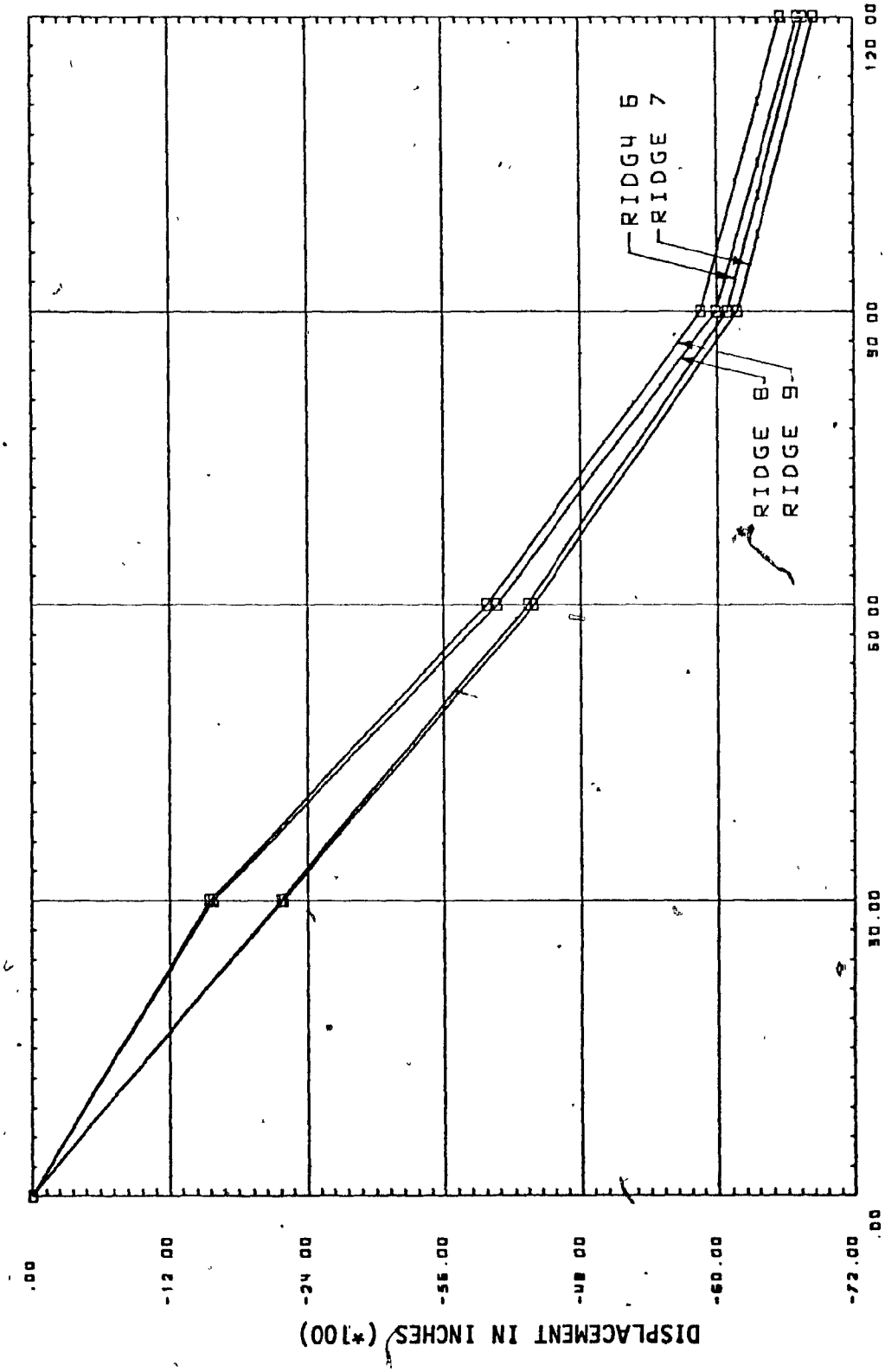

FIG. 5.4 FOLD LINE DEFORMED SHAPE OF FOLD 2

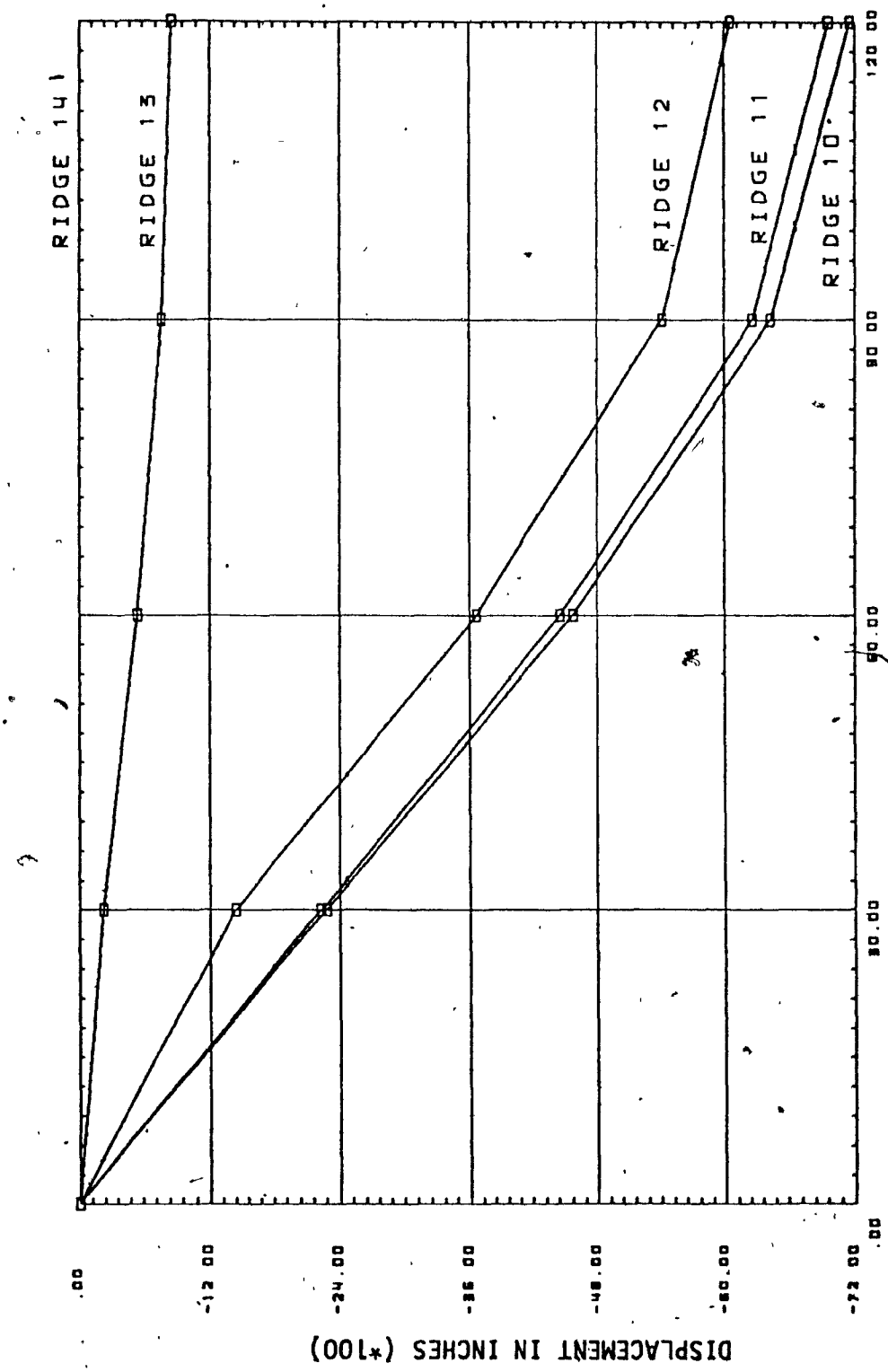

FIG. 5.5 FOLD LINE DEFORMED SHAPE OF FOLD 3

the ridges bracing the glazings is of the order of .001 inch which can be taken up by the cushioning pad placed between the glazings and the framing extrusions. Fig. 5.6 shows the deformed geometry at the midspan section of the roof. The maximum fold line displacement is off from the centre and it occurs at node No. 66. This is due to the unsymmetrical geometry of the fold section. The maximum displacement is 1/340 of the span length of the roof. The results obtained from the analysis are conservative, because the glazing area is treated as openings.

The maximum principal stress is observed at node no. 23, and its magnitude is -4236.40 psi (29.21 M Pa). The maximum bending stress is observed at node no. 67 and its magnitude is - 1991.45 psi (13.73 M Pa). The distribution of longitudinal stress on the top facing (including both bending and membrane action) at the midspan section is shown in Fig. 5.7. Since the glazings are treated as openings, the stress distribution cannot be evaluated over the glazing area and hence is not shown in the figure.

(i) Effect of shear modulus of core on maximum deflection:

A set of analyses has been done by varying the shear modulus of the core over a range of 20 psi (137.9 K Pa) to 2000 psi (13.79 M Pa). The change in maximum displacement which always occured at node no. 66 is shown in Fig. 5.8. It can be observed that the stiffness of the structure increases rapidly with increase in shear modulus within the range of 20 psi (137.9 K Pa) to 420 psi (2.895 M Pa). Increasing the shear

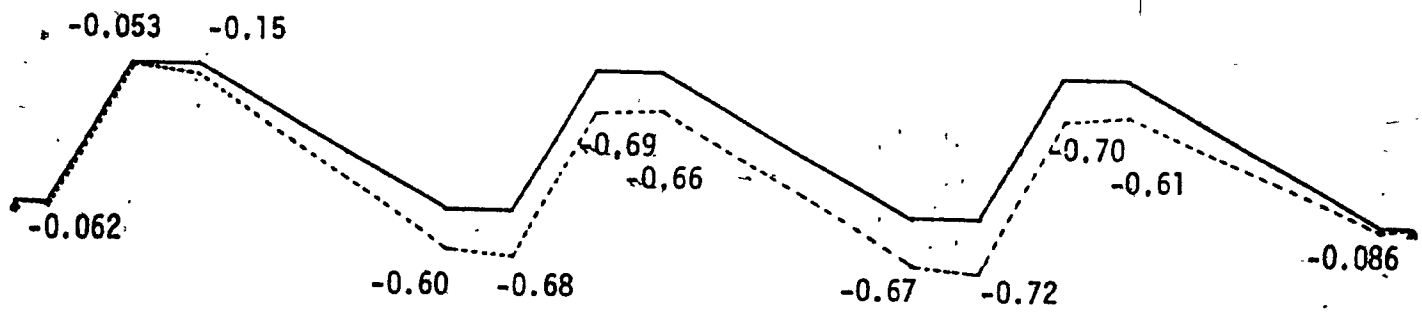

FIG. 5.6 DEFLECTED SHAPE AT MID-SPAN SECTION (IN INCHES)

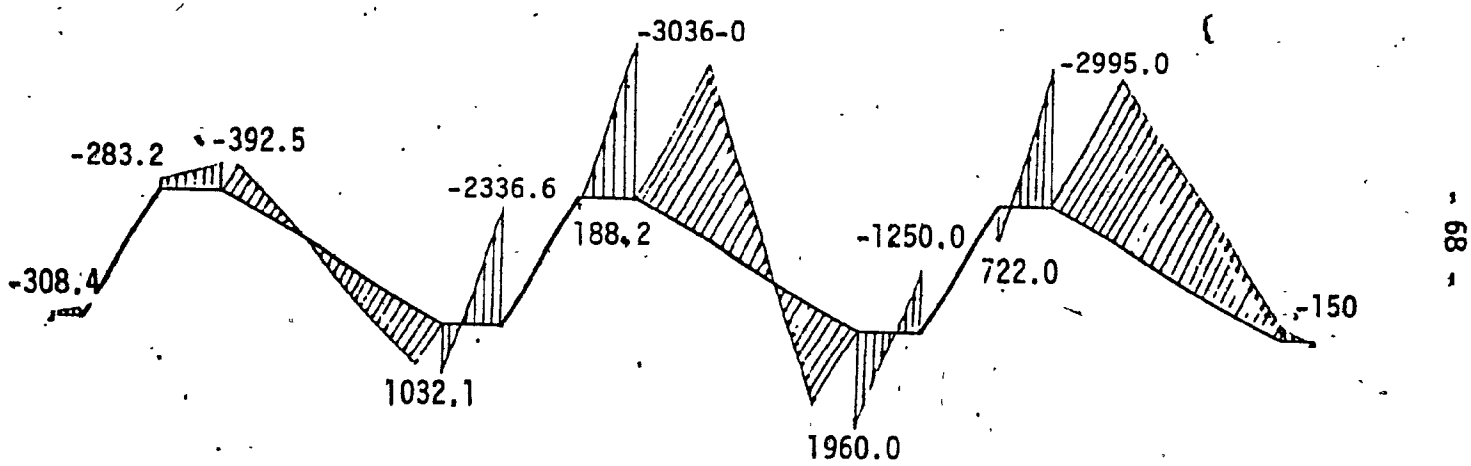

FIG. 5.7 LONGITUDINAL STRESSES (IN PSI) IN TOP FACING AT MIDSPAN SECTION

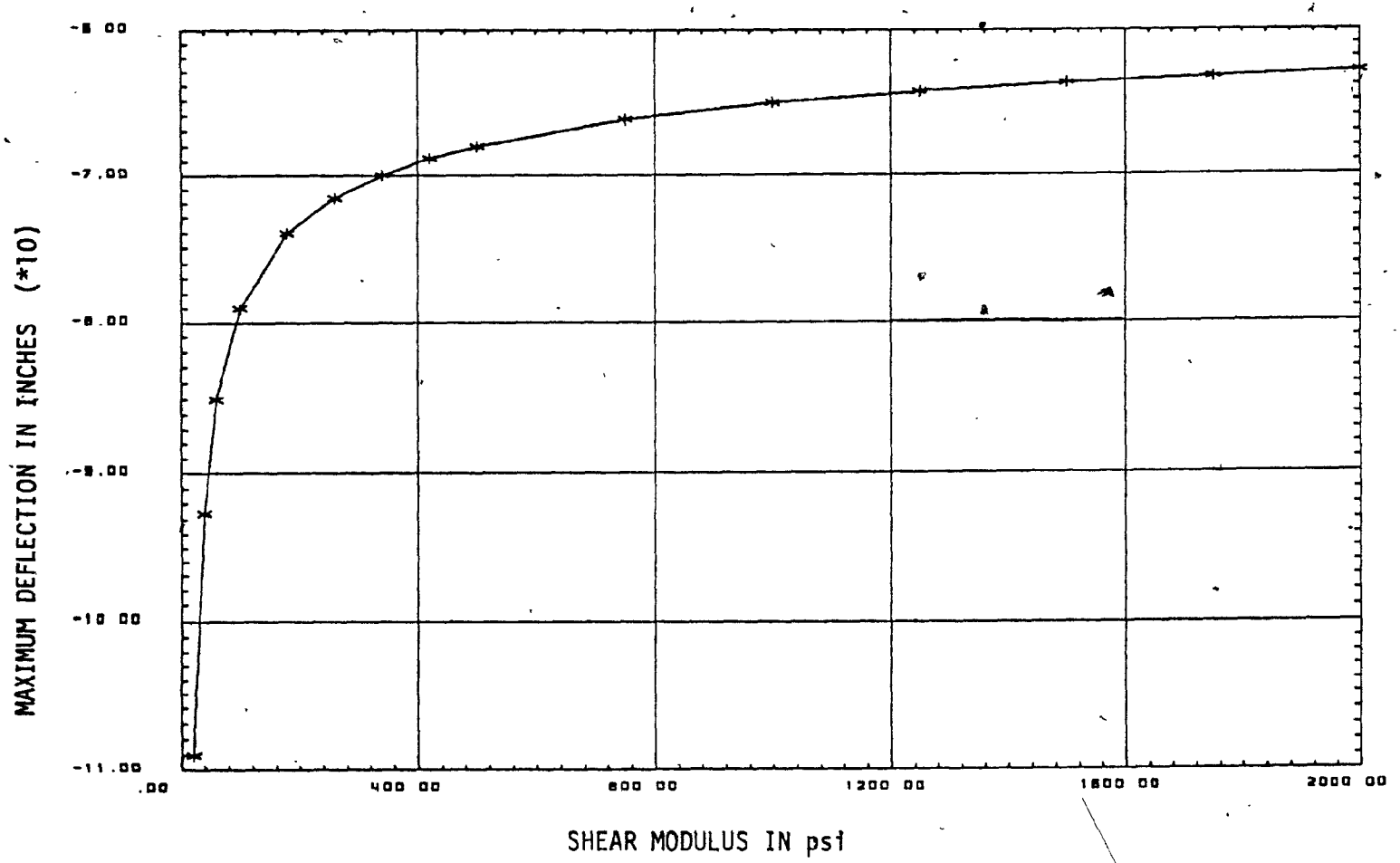

FIG. 5.8 EFFECT OF SHEAR MODULUS OF CORE ON MAXIMUM DEFLECTION

modulus from 420 psi to 2000 psi has very little significance on the increase in resistance offered by the core.

ii) Effect of Elastic Modulus of Facings on Maximum Deflection:

The roof structure has been analyzed for various values of elastic modulus of facing. The change in maximum deflection due to variation in the elastic modulus is shown in Fig. 5.9. It can be seen that increasing the elastic modulus within the range 5×10^6 (34.475 M Pa) psi to 25×10^6 (172.375 M Pa) psi increases the stiffness offered by facings. Increasing the elastic modulus beyond this range does not improve the resistance to maximum deflection.

iii) Effect of Thickness of Core on Maximum Deflection:

Another set of analysis has been performed by varying the thickness of core from 0.5 inch (12.7 mm) to 3.25 inches (82.55 mm). The change in maximum displacement due to this variation is shown in Fig. 5.10. It can be observed that the maximum deflection decreases almost linearly with the increase in the thickness of core. It is obvious that the increase in core thickness separates the facings by a large amount resulting in a higher lever arm and this increases the bending rigidity of the panel.

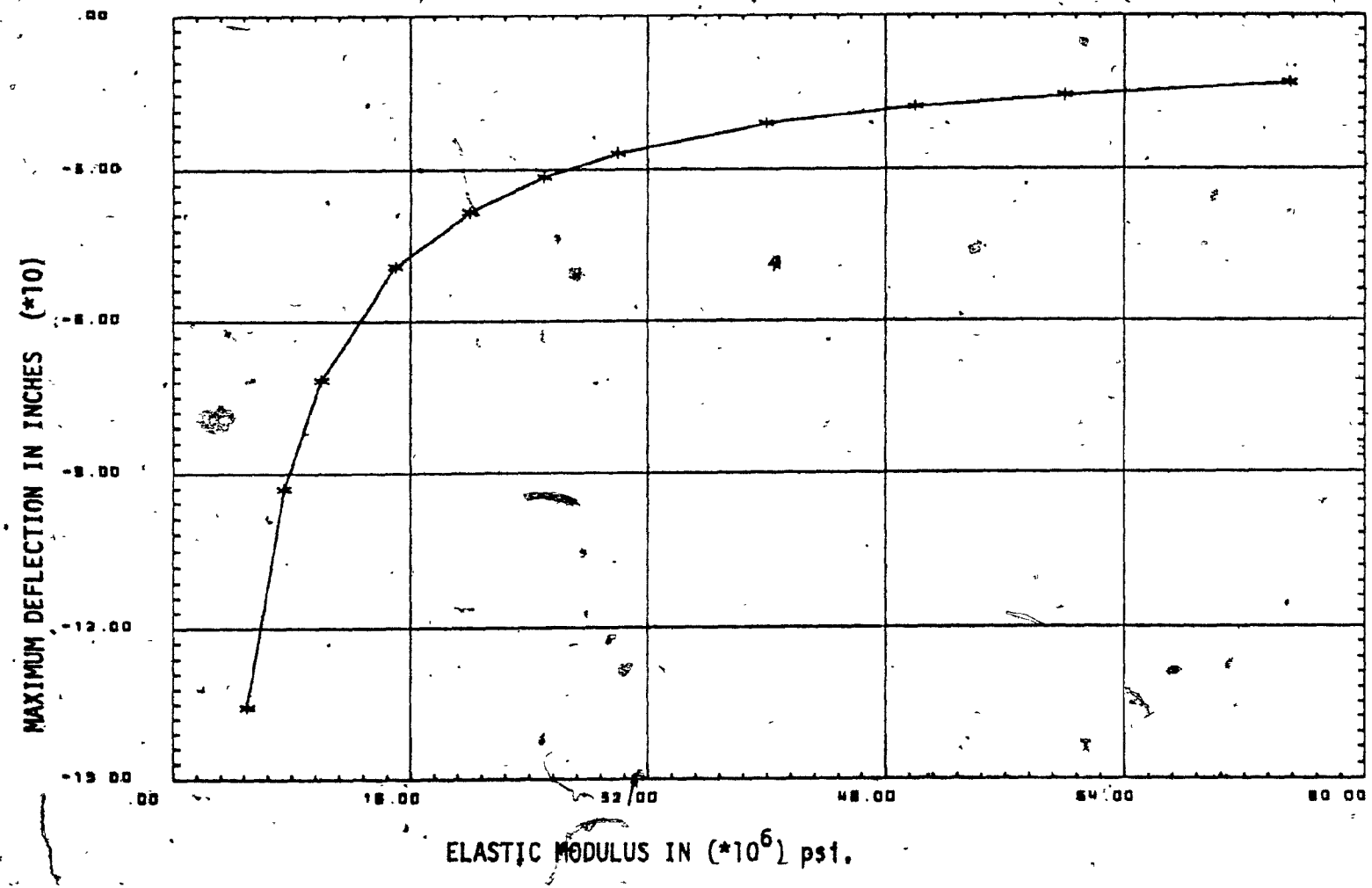

FIG. 5.9 EFFECT OF ELASTIC MODULUS OF FACINGS ON MAXIMUM DEFLECTION

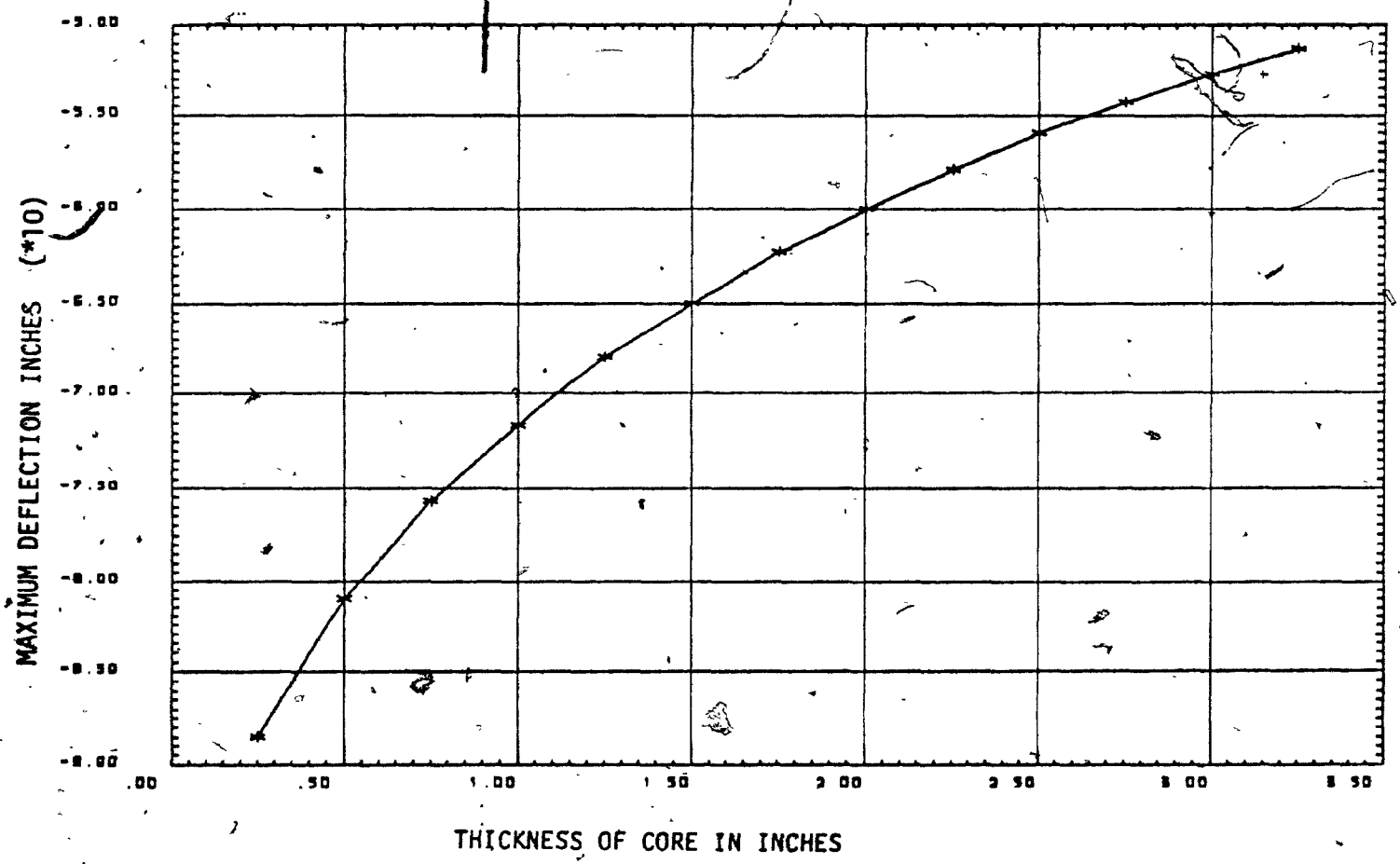

FIG. 5.10 EFFECT OF THICHNESS OF CORE ON MAXIMUM DEFLECTION

iv) Effect of thickness of Facings on Maximum Deflection

This set of analysis has been performed to study the change in maximum displacement due to the variation in thickness of facings. The thickness of facings has been varied over a range of 0.010 inch (0.254 mm) to 0.2 inch (5.08 mm). It can be observed from Fig. 5.11 that there is a rapid increase in the resistance against maximum displacement due to the increase in the thickness of facing within the range of 0.010 to 0.1 inch (2.54 mm). Beyond which the effect of increase in thickness of facing is not very significant.

It has been observed that doubling the thickness of facing decreases the maximum deflection by 30.0%, whereas doubling the thickness of core results only in a 16.2% decrease in the maximum deflection. It should be noted that the core resists only transverse shear deformation, but the faces resist both bending and in-plane stresses.

v) Effect of Span Length on Maximum Deflection

The span of the roof has been varied from 10 ft. (3048 m) to 30 ft. (9.144 mm), with the cross section geometry as in Fig. 5.1. The computed maximum deflection for various span lengths within the range of 10 ft. to 30 ft. is plotted in Fig. 5.12. It can be seen that the increase in span length has a significant increase in maximum deflection, which is obvious. It should be noted that the rate of increase of maximum deflection is increasing with the increase in span length.

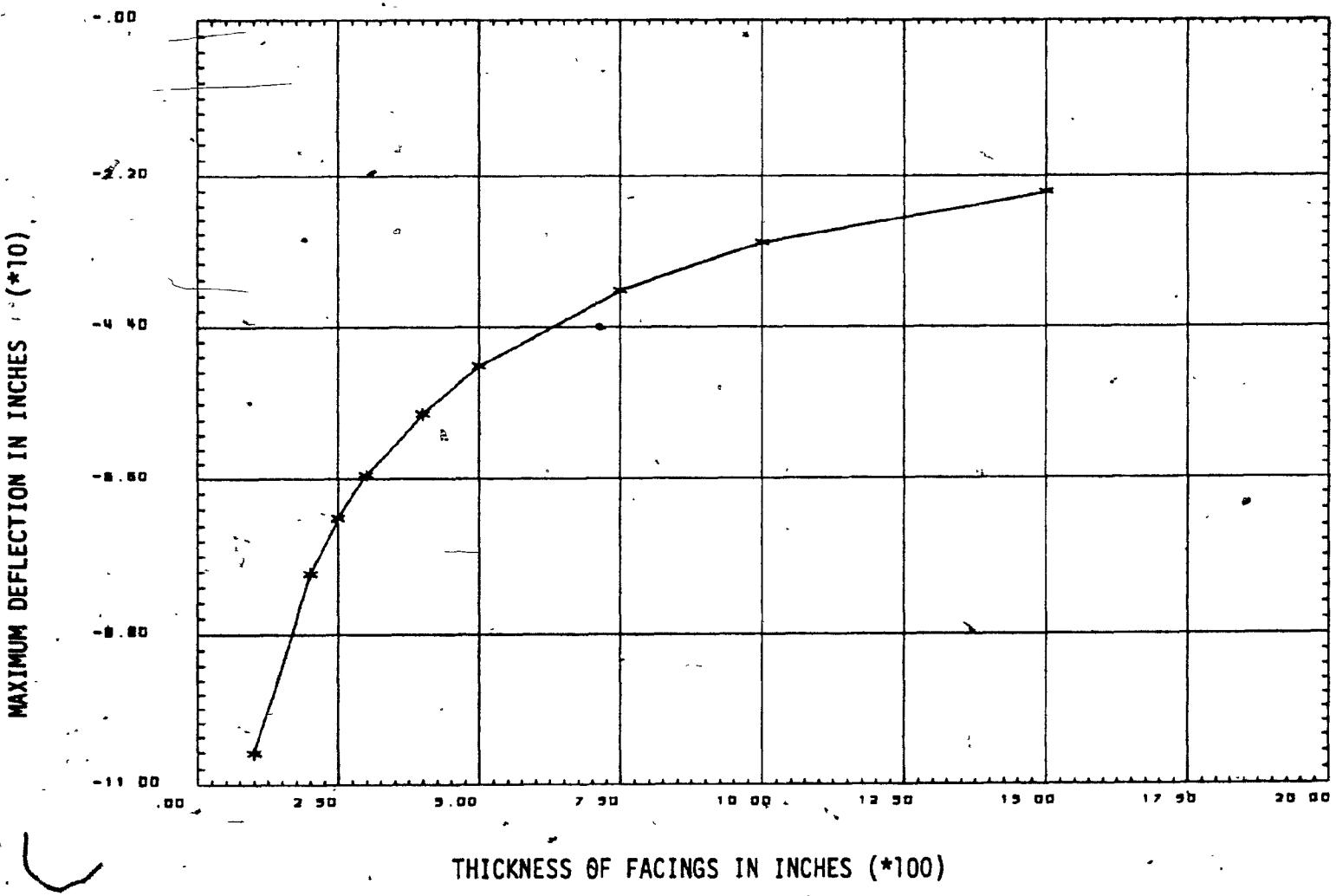

FIG. 5.11 EFFECT OF THICKNESS OF FACINGS ON MAXIMUM DEFLECTION

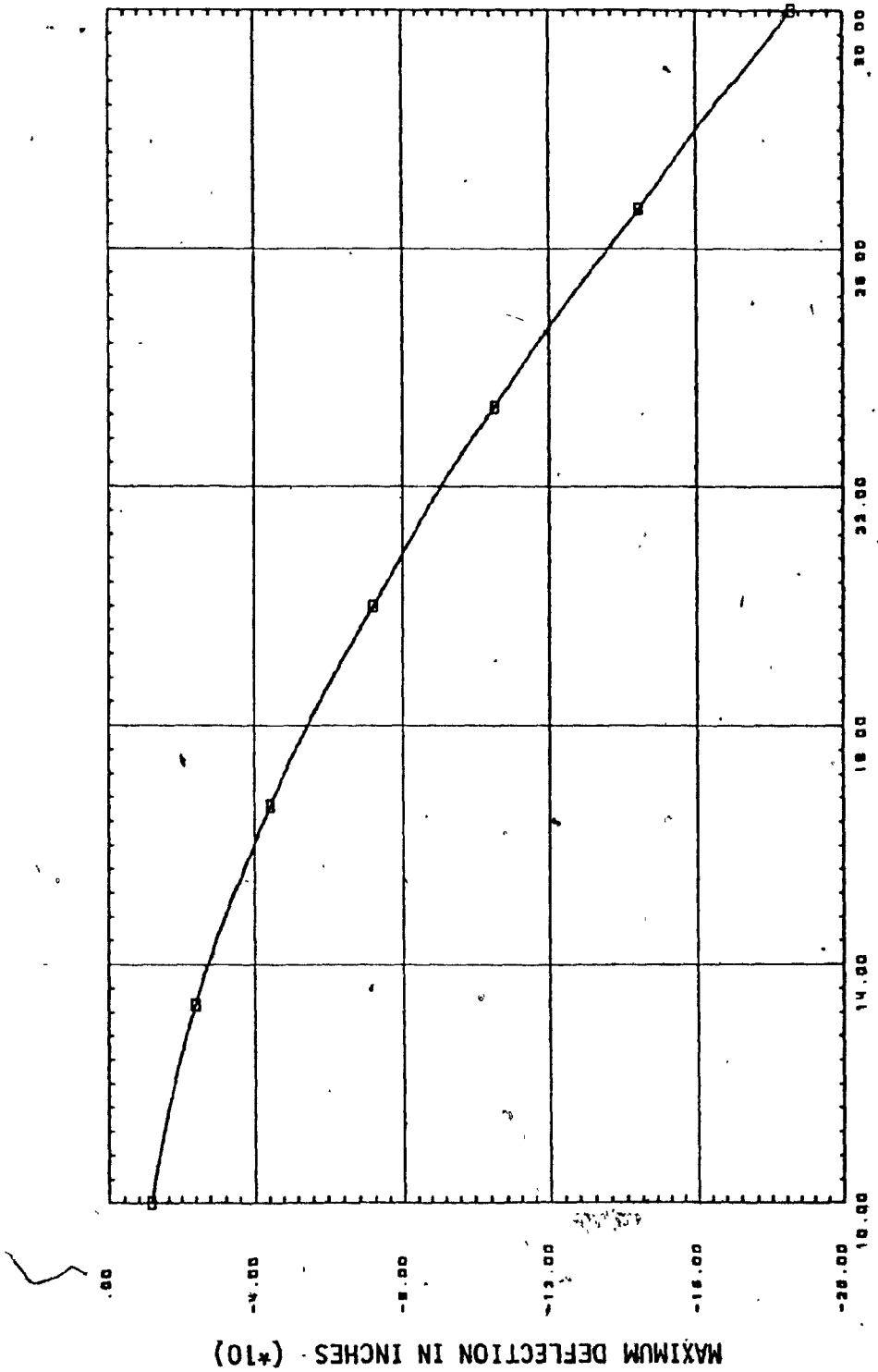

FIG. 5.12 EFFECT OF SPAN LENGTH ON MAXIMUM DEFLECTION

vi) Effect of Number of Folds on Maximum Deflection

The number of folds of the roof has been varied from two to eight with the same fold geometry and span as in Fig. 5.1. The maximum deflection corresponding to the various number of folds are shown in Fig. 5.13. The roof becomes more flexible with the increase in the number of folds. But the rate of increase diminishes with the increase in the number of folds. The maximum deflection for an eight fold roof covering an area of 560 sq. ft. is 0.8710 inch (22 mm) which is 1/275 of the span length.

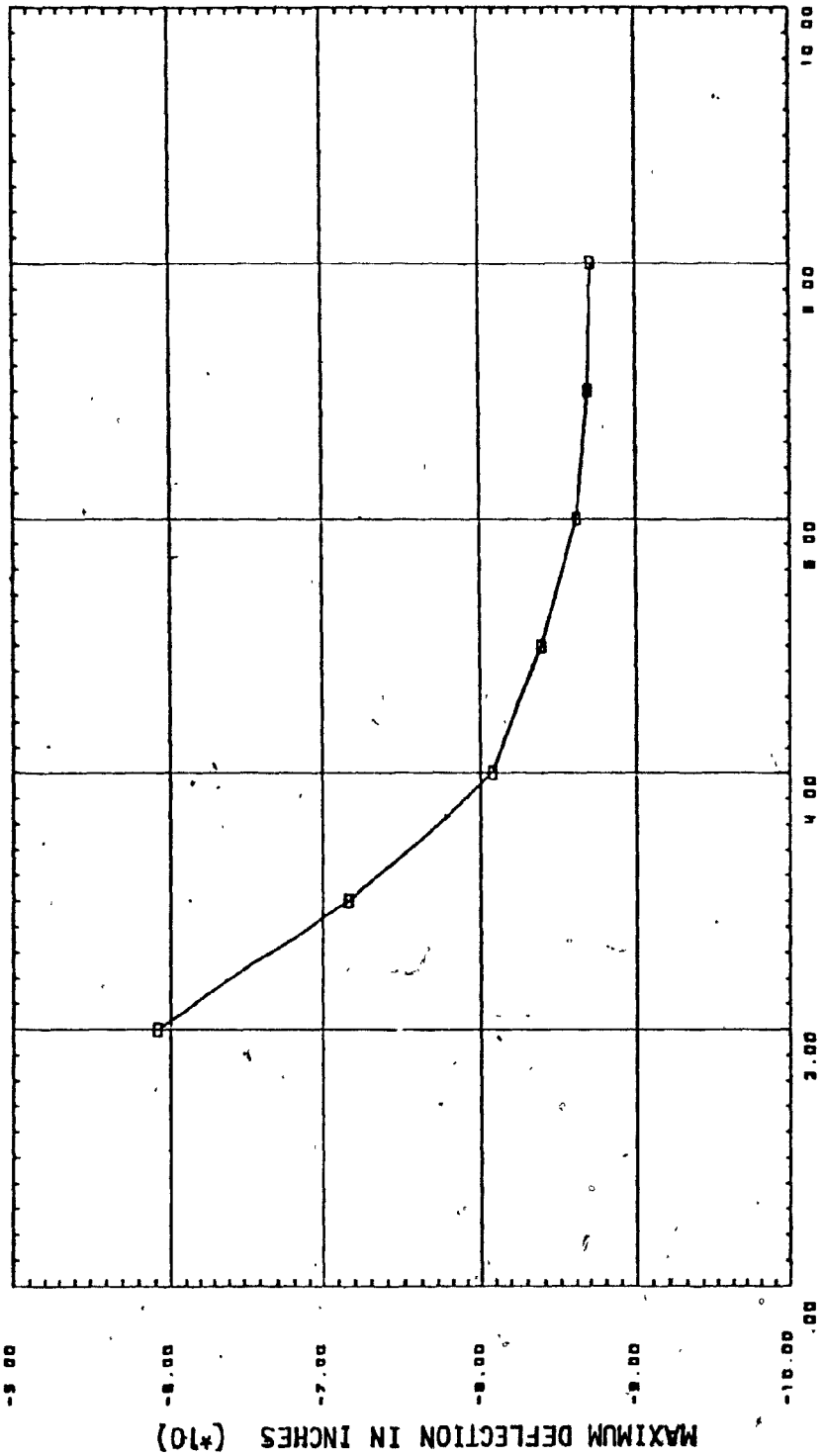

FIG. 5.13 EFFECT OF NUMBER OF FOLDS ON MAXIMUM DEFLECTION

CHAPTER VI

CONCLUSION

The investigation reported in this study deals with the development of an integrated, energy efficient passive solar roofing system and its structural analysis. The present research has resulted in the formulation of simpler rectangular assumed stress hybrid finite elements for the three dimensional analysis of sandwich plate structures. The following conclusions can be drawn on the basis of the work reported in this investigation:

i) The geometry of folded plate roof can be chosen to integrate passive solar glazings which will provide natural daytime illumination and winter space heating energy for single storey commercial and industrial buildings.

ii) Sandwich panels can be used for roofing. These panels have satisfactory structural performance and can satisfy the required thermal insulation standard.

iii) Rectangular assumed stress hybrid finite elements can be conveniently used for the analysis of complex sandwich plate structures. Since the elements possess only geometrical degrees of freedom such as displacements and rotations, no difficulties arise due to the transformation of the generalized forces and displacements along the joints.

iv) In the rectangular assumed stress hybrid elements with linear edge variations, simpler assumed stress modes are found to perform better when compared to higher order assumed stress modes. Use of a simpler stress function results in the reduction of the size of matrices to be used, length of the program and the computation time for the generation of an element stiffness matrix.

v) The load-deformation characteristics of the analytical roof model are within the serviceability limits. The structural performance of the roofing system can be improved by increasing the thickness of facings and core. Also, increasing the shear rigidity of core and elastic modulus of facings will result in an increased stiffness offered by the structural system.

vi) The maximum vertical deflection of the roof increases with an increase in the span of the roof and with an increase in the number of folds.

CHAPTER VII

RECOMMENDATIONS FOR FUTURE STUDY

1. A prototype model with glazings can be tested in the laboratory to study the structural behaviour. The results of such an experimental test can be compared to that of the finite element analysis.

2. Different fold geometries with various inclination of glazing panels have to be investigated.

3. Detailed energy analysis can be performed to study the viability of integrated passive roof systems for use in single storey industrial and commercial buildings.

4. The effect of the ratio of the glazing area to that of the building area has to be investigated.

5. Design details for connecting the glazing panels with the roofing sandwich panels along the fold lines should be investigated.

REFERENCES

(1) Anderson, B. and Wells, M., "Passive Solar Energy: The Home Owners' Guide to Natural Heating and Cooling", Brick House Pub. Co., 1981, p. 114.

(2) Balcomb, J.D. et al, "Research on Integrated Solar Collector Roof Structures", Report No. LA-UR-75-1335, presented at the International Solar Energy Congress and Exposition, UCLA Campus, July 28 - Aug. 1, 1975, pp. 12.

(3) Barnard, A.J., "A Sandwich Plate Finite Element", The Mathematics of Finite Elements and Applications, Proceedings of the Brunel University Conference of the Institute of Mathematics and its Applications, held in April 1972, J.R. Whiteman (ed.), Academic Press, London, 1973, pp. 401-413.

(4) Beavers, J.E. and Beaufit, F.W., "Higher Order Finite Elements for Complex Plate Structures", J. of Struct. Div., ASCE, Vol. 103, No. ST 1, Jan. 1977, pp. 51-69.

(5) Comstock, W.S., "TRENDS: Commercial/Industrial Applications Spur Solar Development", ASHRAE Journal Nov. 1977, p. 32.

(6) Cook, R.D., "Two Hybrid Elements for Analysis of Thick, Thin and Sandwich Plates", International Journal for Numerical Methods in Engineering, Vol. 5, 1972, pp. 272-288.

(7) Cook, R.D., "Some Elements for the Analysis of Plate Bending", J. of Engineering Mechanics Div., ASCE, Vol. 98, No. EM6, December 1972, pp. 1453-1470.

(8) Cook, R.D. and Ladkany, S.G., "Observations Regarding Assumed Stress Hybrid Plate Elements", International Journal for Numerical Methods in Engineering, Vol. 8, 1974, pp. 513-519.

(9) Cook, R.D., "Concepts and Applications of Finite Element Analysis", Second Edition, J. Wiley and Sons Inc., 1981, pp. 537.

(10) De Fries-Skene, A., and Scordelis, A.C., "Direct Stiffness Solution for Folded Plates", J. of Struct. Div., ASCE, Vol. 90, No. ST4, Aug. 1964, pp. 15-49.

(11) Eggers-Lura, A., "Solar Energy in Developing Countries", TJ 810, E355, PSEL Library, McGill University, 1979, pp. 27-34.

(12) Fazio, P. and Kennedy, J.B., "Experimental and Theoretical Study of Aluminium Sandwich Elements - in Particular Aluminium Folded Sandwich Plate Structures", TA 660, P6 F3, Concordia University Libraries, June 1968.

(13) Fazio, P. and Dewall, J.F., "An Elasticity Theory for the Analysis of Prismatic Folded Sandwich Plate Structures", Report No. SBC - 22, CE 71-4, June 1971, Department of Civil Engineering, Sir George Williams University, Montreal, Canada, pp. 90.

(14) Fazio, P., "Failure Modes of Folded Sandwich Panel Roofs", J. of Struct. Div. ASCE, Vol. 98, No. ST5, May 1972, pp. 1085-1104.

(15) Fazio, P. and Ha, H.K., "Sandwich Plate Structure Analysis by Finite Element", J. of Struct. Div. ASCE, Vol. 100, No. ST6, June 1974, pp. 1243-1262.

(16) Folie, G.M., "Stiffness Matrix for Sandwich Folded Plates", J. of Struct. Div., ASCE, Vol. 97, No. ST. 2, Feb. 1971, pp. 603-617.

(17) Givoni, B., "Conservation and the Use of Integrated - Passive Energy Systems in Architecture", Energy and Buildings, 3(1981), pp. 213-228.

(18) Goldberg, J.E. and Leve, H.L., "Theory of Prismatic Folded Plate Structures", IABSE, Vol. No. 17, 1957, pp. 59-86.

(19) Gowri, K. and Fazio, P., "Program for Finite Element Analysis of Sandwich Plate Structures: Instructions to User", Report No. CBS-108, Centre for Building Studies, Concordia University, Feb. 1984.

(20) Ha, H.K. and Fazio, P., "Analysis of Three Dimensional Orthotropic Sandwich Plate Structure by Finite Element Method", Report No. - SBC - 72 - 20, CBS, Concordia University, (1972), pp. 134.

(21) Ha, H.K., and Fazio, P., "Flexural Behaviour of Sandwich Floor Assembly", Building and Environment, Vol. 13, pp. 61-67, 1978.

(22) Hastings, S.R., "Passive Solar Design for Urban Commercial Environments", 4th National Passive Solar Energy Conference, Kansas City, Missouri, 3-5 Oct., 1979, pp. 303-306.

(23) Jafari-Naini, B., "Comparative Study on Sandwich Plate Finite Elements", M.Eng. Thesis to be Submitted to the Centre for Building Studies, Concordia University, 1984.

(24) Nilson, A.H., "Folded Plate Structures of Light Gauge Steel", J. of Struct. Div. ASCE, Vol. 87, No. ST7, Oct. 1961, pp. 215-237.

(25) Passive Solar Design Hand Book, Volume I and II, U.S. Department of Energy, DOE/CS-0127/1 and 2, March 1980.

(26) Pian, T.H.H., "Element Stiffness Matrices for Boundary Compatibility and for Prescribed Boundary Stresses", Proceedings of First Conference on Matrix Methods in Structural Mechanics, Wright - Patterson Airforce Base, Ohio, AFFDL-TR-66-80, 1966, pp. 457-477.

(27) Pian, T.H.H. and Tong, P., "Rationalization in Deriving Element Stiffness Matrix by Assumed Stress Approach", Proceedings of Second Conference on Matrix Methods in Structural Mechanics, Wright - Patterson Airforce Base, Ohio, AFFDL-TR-68-150, 1968, pp. 441-469.

(28) Pian, T.H.H. and Mau, S.T., "Some Recent Studies in Assumed Stress Hybrid Models", Advances in Computational Methods in Structural Mechanics and Design (Eds: J.T. Oden, R.W. Clough and Y. Yamamoto), University of Alabama press, Alabama, 1972, pp. 87-106.

(29) Place, W. et al, "Roof Apertures in Office Buildings", LBL - 14790, Presented at the 1983 International Daylighting Conference, Phoenix, Az., Feb. 16-18, 1983, pp. 13.

(30) Plantema, F.J., "Sandwich Construction (The bending and buckling of sandwich beams, plates and shells)", John Wiley and Sons, N.Y. (1966), pp. 246.

(31) Shapira, H.B. and Barnes, P.R., "RIB - Reflective Insulating Blinds", Presented at the Fourth National Passive Solar Energy Conference, Kansas City, Missouri, 3-5 Oct. 1979, pp. 393-394.

(32) Shurcliff, W.A., "Solar Heated Buildings of North America: 120 Outstanding Examples", Brick House Publishing Co., pp. 198-201.

(33) Vinckier, A.G. and Vanleathem, M., "Folded Plate Roofs Made with Wood and Plywood Sandwich Panels", Bulletin of the International Association of Shell and Spatial Structures, Vol. XXI-3, pp. 11-15.

APPENDIX - A

Procedure for the formulation of stiffness matrix by assumed stress hybrid technique.

Step: 1. Assume stress distributions in the element

$$\{\sigma\} = [P]\{\beta\} \qquad (A.1)$$

where $\{\sigma\}$: generalized stress vector, must satisfy the equilibrium conditions.

$\{\beta\}$: undetermined stress parameters.

$[P]$: functions of the coordinates.

Step: 2. Evaluate the strain energy in terms of stress parameters

$$U = \tfrac{1}{2}\{\beta\}^T [H]\{\beta\} \qquad (A.2)$$

The matrix $[H]$ may be determined directly from the strain energy expression or as follows:

Stress-Strain Relation

$$\{\varepsilon\} = [N]\{\sigma\} \qquad (A.3)$$

Strain Energy $U = \tfrac{1}{2}\int_V \{\sigma\}^T\{\varepsilon\}\, dV$

Substitution of $\{\varepsilon\}$ from eqn. (A.3) and $\{\sigma\}$ from eqn. (A.1) into the above equation yields:

$$U = \tfrac{1}{2}\int_V \{\beta\}^T[P]^T[N]\,[P]\{\beta\}\, dV$$

$$= \tfrac{1}{2}\{\beta\}^T \int_V [P]^T[N]\,[P]\, dV\, \{\beta\}$$

Then

$$[H] = \int_V [P]^T[N][P]dV \qquad (A.4)$$

Matrix $[H]$ is positive, definite and symmetric.

Step 3: Introduce the generalized edge displacements

$$\{u\} = [L]\{q\} \tag{A.5}$$

where

$\{q\}$: generalized nodal displacements.

$\{L\}$: functions of the coordinates.

By chosing suitable interpolation functions for [L] the displacement compatibility along the element boundaries can be achieved.

Step 4: From the generalized edge forces $\{S\}$ in terms of $\{\beta\}$ by using (A.1).

$$\{S\} = [R]\{\beta\}$$

The coefficients in $\{S\}$ should correspond to those in $\{u\}$ so that the work done by the edge forces is given by the expression

$$W = \phi \{S\}^T\{u\}ds$$

$$= \phi \{\beta\}^T[R]^T[L]\{q\}ds$$

$$= \{\beta\}^T[T]\{q\} \tag{A.6}$$

where

$$[T] = \phi [R]^T[L]ds$$

The vector $\{Q\}$ of nodal generalized forces is defined by

$$\{Q\}^T\{q\} = W = \{\beta\}^T[T]\{q\}$$

or

$$\{Q\} = [T]^T\{\beta\} \qquad (A.7)$$

Step 5: Form the total complementary energy

$$\Pi_c = U - W = \tfrac{1}{2}\ \{\beta\}^T[H]\{\beta\} - \{\beta\}^T[T]\{q\}$$

The principle of stationary complementary energy requires that

$$\frac{\partial \Pi_c}{\partial\{\beta\}} = [H]\{\beta\} - [T]\{q\} = 0$$

Hence

$$\{\beta\} = [H]^{-1}\ [T]\{q\} \qquad (A.8)$$

Step 6:

The stiffness matrix [K] is given by

$$\{Q\} = [K]\{q\} \qquad (A.9)$$

Using eqns. (A.7) and (A.8)

$$[K]\{q\} = [T]^T[H]^{-1}[T]\{q\}$$

Then

$$[K] = [T]^T[H]^{-1}[T] \qquad (A.10)$$

APPENDIX B

Matrices Used in the Derivation of the Stiffness Matrix for RH11B Element

$$\begin{bmatrix} 1 & 0 & 0 & \bar{x} & 0 & 0 & \bar{y} & 0 & 0 & \bar{xy} & 0 \\ 0 & 1 & 0 & 0 & \bar{x} & 0 & 0 & \bar{y} & 0 & 0 & \bar{xy} \\ 0 & 0 & 1 & 0 & 0 & \bar{x} & 0 & 0 & \bar{y} & 0 & 0 \\ 0 & 0 & 0 & 1/a & 0 & 0 & 0 & 0 & 1/b & \bar{y}/a & 0 \\ 0 & 0 & 0 & 0 & 0 & 1/a & 0 & 1/b & 0 & 0 & \bar{x}/b \end{bmatrix}$$

(i) Matrix [P] in the relation $\{\sigma\} = [P]\{\beta\}$

$$\begin{bmatrix} 1/B & -\gamma/B & 0 & 0 & 0 \\ -\gamma/B & 1/B & 0 & 0 & 0 \\ 0 & 0 & \frac{2(1+\gamma)}{B} & 0 & 0 \\ 0 & 0 & 0 & 1/S & 0 \\ 0 & 0 & 0 & 0 & 1/S \end{bmatrix}$$

where $B = \frac{Etd^2}{2}$ and

$$S = \frac{Gd^2}{h}$$

(ii) Matrix [N] in the relation $\{\sigma\} = [N]\{\varepsilon\}$

$$\frac{ab}{B}\begin{bmatrix}
1 & -\gamma & 0 & 1/2 & -\gamma/2 & 0 & 1/2 & -\gamma/2 & 0 & 1/4 & -\gamma/4 \\
 & 1 & 0 & -\gamma/2 & 1/2 & 0 & -\gamma/2 & 1/2 & 0 & -\gamma/4 & 1/4 \\
 & & 2(1+\gamma) & 0 & 0 & 1+\gamma & 0 & 0 & (1+\gamma) & 0 & 0 \\
 & & & \frac{1}{3}+\frac{B}{Sa^2} & -\gamma/3 & 0 & 1/4 & -\gamma/4 & \frac{B}{Sab} & \frac{1}{6}+\frac{B}{2Sa^2} & -\gamma/6 \\
 & & & & 1/3 & 0 & -\gamma/4 & 1/4 & 0 & -\gamma/6 & 1/6 \\
 & & & & & \frac{2(1+\gamma)}{3}+\frac{B}{Sa^2} & 0 & \frac{B}{Sab} & \frac{(1+\gamma)}{2} & 0 & \frac{B}{2sab} \\
 & & & & & & 1/3 & -\gamma/3 & 0 & 1/6 & \gamma/6 \\
 & & & & & & \frac{1}{3}+\frac{B}{Sb^2} & 0 & & -\gamma/6 & \frac{1}{6}+\frac{B}{2sb^2} \\
 & & & & & & & \frac{2(1+\gamma)}{3}+\frac{B}{Sb^2} & \frac{B}{2sab} & 0 & \\
 & & & & & & & & \frac{1}{9}+\frac{B}{3sa^2} & -\frac{\gamma}{9} & \\
 & & & & & & & & & \frac{1}{9}+\frac{B}{3sb^2} &
\end{bmatrix}$$

(iii) Matrix $[H] = \int_{Vol} [P]^T [N] [P] \, dv.$

$$
\begin{bmatrix}
0 & -1 & 0 & 0 & -\bar{x} & 0 & 0 & 0 & 0 & 0 & 0 \\
0 & 0 & -1 & 0 & 0 & -x & 0 & 0 & 0 & 0 & 0 \\
0 & 0 & 0 & 0 & 0 & -1/a & 0 & -1/b & 0 & 0 & -\bar{x}/b \\
0 & 1 & 0 & 0 & \bar{x} & 0 & 0 & \bar{y} & 0 & 0 & \overline{xy} \\
0 & 0 & 1 & 0 & 0 & x & 0 & 0 & \bar{y} & 0 & \\
0 & 0 & 0 & 0 & 0 & 1/a & 0 & 1/b & 0 & 0 & \bar{x}/b \\
0 & 0 & -1 & 0 & 0 & 0 & 0 & 0 & -\bar{y} & 0 & 0 \\
-1 & 0 & 0 & 0 & 0 & 0 & -\bar{y} & 0 & 0 & 0 & 0 \\
0 & 0 & 0 & -1/a & 0 & 0 & 0 & 0 & -1/b & -\bar{y}/a & 0 \\
0 & 0 & 1 & 0 & 0 & \bar{x} & 0 & 0 & \bar{y} & 0 & 0 \\
1 & 0 & 0 & \bar{x} & 0 & 0 & \bar{y} & 0 & 0 & \overline{xy} & 0 \\
0 & 0 & 0 & 1/a & 0 & 0 & 0 & 0 & 1/b & \bar{y}/a & 0
\end{bmatrix}
$$

(iv) Matrix [R] in the relation

$$[S] = [R] \{\beta\}$$

$$
\begin{bmatrix}
1-\bar{x} & 0 & 0 & \bar{x} & 0 & 0 & 0 & 0 & 0 & 0 & 0 & 0 \\
0 & 1-\bar{x} & 0 & 0 & \bar{x} & 0 & 0 & 0 & 0 & 0 & 0 & 0 \\
0 & 0 & 1-\bar{x} & 0 & 0 & \bar{x} & 0 & 0 & 0 & 0 & 0 & 0 \\
0 & 0 & 0 & 0 & 0 & 0 & 1-\bar{x} & 0 & 0 & \bar{x} & 0 & 0 \\
0 & 0 & 0 & 0 & 0 & 0 & 0 & 1-\bar{x} & 0 & 0 & \bar{x} & 0 \\
0 & 0 & 0 & 0 & 0 & 0 & 0 & 0 & 1-\bar{x} & 0 & 0 & \bar{x} \\
1-\bar{y} & 0 & 0 & 0 & 0 & 0 & \bar{y} & 0 & 0 & 0 & 0 & 0 \\
0 & 1-\bar{y} & 0 & 0 & 0 & 0 & 0 & \bar{y} & 0 & 0 & 0 & 0 \\
0 & 0 & 1-\bar{y} & 0 & 0 & 0 & 0 & 0 & \bar{y} & 0 & 0 & 0 \\
0 & 0 & 0 & 1-\bar{y} & 0 & 0 & 0 & 0 & 0 & \bar{y} & 0 & 0 \\
0 & 0 & 0 & 0 & 1-\bar{y} & 0 & 0 & 0 & 0 & 0 & \bar{y} & 0 \\
0 & 0 & 0 & 0 & 0 & 1-\bar{y} & 0 & 0 & 0 & 0 & 0 & \bar{y}
\end{bmatrix}
$$

(v) Matrix [L] in the relation {u} = [L] {q}

u: generalized edge displacements
q: nodal displacements

$$
\begin{bmatrix}
0 & -b/2 & 0 & 0 & b/2 & 0 & 0 & -b/2 & 0 & 0 & b/2 & 0 \\
-a/2 & 0 & 0 & -a/2 & 0 & 0 & a/2 & 0 & 0 & a/2 & 0 & 0 \\
-a/2 & -a/2 & 0 & b/2 & -a/2 & 0 & -b/2 & a/2 & 0 & b/2 & a/2 & 0 \\
0 & 0 & -b/2a & 0 & b/2 & b/2a & 0 & 0 & -b/2a & 0 & b/2 & b/2a \\
-a/6 & 0 & 0 & -a/3 & 0 & 0 & a/6 & 0 & 0 & a/3 & 0 & 0 \\
0 & -a/6 & -1/2 & b/2 & -a/3 & -1/2 & 0 & a/6 & 1/2 & b/2 & a/3 & 1/2 \\
0 & -b/6 & 0 & 0 & b/6 & 0 & 0 & -b/3 & 0 & 0 & b/3 & 0 \\
0 & 0 & -a/2b & 0 & 0 & -a/2b & a/2 & 0 & a/2b & a/2 & 0 & a/2b \\
-b/6 & 0 & -1/2 & b/6 & 0 & 1/2 & -b/3 & a/2 & -1/2 & b/3 & a/2 & 1/2 \\
0 & 0 & -b/6a & 0 & b/6 & b/6a & 0 & 0 & -b/3a & 0 & b/3 & b/3a \\
0 & 0 & -a/6b & 0 & 0 & -a/3b & a/6 & 0 & a/6b & a/3 & 0 & a/3b
\end{bmatrix}
$$

(vi) Matrix $[T] = [R]^T[L]$ ds.

APPENDIX C

Matrices Used in the Derivation of The Stiffness Matrix for RH7M Element

$$\begin{bmatrix} 1 & \bar{x} & \bar{y} & 0 & 0 & 0 & 0 \\ 0 & 0 & 0 & 1 & \bar{x} & \bar{y} & 0 \\ 0 & \frac{-b}{a}\bar{y} & 0 & 0 & 0 & \frac{-a}{b}\bar{x} & 1 \end{bmatrix}$$

(i) Matrix [P] in the relation $\{\sigma\} = [P]\{\beta\}$.

$$\begin{bmatrix} 1/E & -\gamma/E & 0 \\ -\gamma/E & 1/E & 0 \\ 0 & 0 & \frac{2(1+\gamma)}{E} \end{bmatrix}$$

(ii) Matrix [N] in the relation $\{E\} = [N]\{\sigma\}$

$$\begin{bmatrix} 1 & 1/2 & 1/2 & -\gamma & -\gamma/2 & -\gamma/2 & 0 \\ & \frac{1}{3}+\frac{2(1+\gamma)b^2}{3a^2} & 1/4 & -\gamma/2 & -\gamma/3 & \frac{(2+\gamma)}{4} & -\frac{b(1+\gamma)}{a} \\ & & 1/3 & -\gamma/2 & -\gamma/4 & -\gamma/3 & 0 \\ & & & 1 & 1/2 & 1/2 & 0 \\ \text{SYMMETRIC} & & & & 1/3 & 1/4 & 0 \\ & & & & & \frac{1}{3}+\frac{2(1+\gamma)a^2}{3b^2} & \frac{-a(1+\gamma)}{b} \\ & & & & & & 2(1+\gamma) \end{bmatrix}$$

(iii) Matrix $[H] = \int_{vol}[P]^T[N][P].\,dv.$

$$\begin{bmatrix} 0 & 0 & 0 & 0 & 0 & \frac{a}{b}\bar{x} & -1 \\ 0 & 0 & 0 & -1 & -\bar{x} & 0 & 0 \\ 1 & 1 & \bar{y} & 0 & 0 & 0 & 0 \\ 0 & -\frac{b}{a}\bar{y} & 0 & 0 & 0 & -a/b & 1 \\ 0 & -\frac{b}{a} & 0 & 0 & 0 & -a/b\,\bar{x} & 1 \\ 0 & 0 & 0 & 1 & \bar{x} & 1 & 0 \\ -1 & 0 & -\bar{y} & 0 & 0 & 0 & 0 \\ 0 & \frac{b}{a}\bar{y} & 0 & 0 & 0 & 0 & -1 \end{bmatrix}$$

(iv) Matrix [R] in the relation [S] = [R] {β}

$$\begin{bmatrix} 1-\bar{x} & 0 & \bar{x} & 0 & 0 & 0 & 0 & 0 \\ 0 & 1-\bar{x} & 0 & \bar{x} & 0 & 0 & 0 & 0 \\ 0 & 0 & 1-\bar{y} & 0 & 0 & 0 & \bar{y} & 0 \\ 0 & 0 & 0 & 1-\bar{y} & 0 & 0 & 0 & \bar{y} \\ 0 & 0 & 0 & 0 & 1-\bar{x} & 0 & \bar{x} & 0 \\ 0 & 0 & 0 & 0 & 0 & 1-\bar{x} & 0 & \bar{x} \\ 1-\bar{y} & 0 & 0 & 0 & \bar{y} & 0 & 0 & 0 \\ 0 & 1-\bar{y} & 0 & 0 & 0 & \bar{y} & 0 & 0 \end{bmatrix}$$

(v) Matrix [L] in the relation {u} = [L] {q}

$$\begin{bmatrix}
-b/2 & 0 & b/2 & 0 & -b/2 & 0 & b/2 & 0 \\
0 & b^2/6a & b/2 & -b^2/6a & -b/2 & b^2/3a & 0 & -b^2/3a \\
-b/6 & 0 & b/6 & 0 & -b/3 & 0 & b/3 & 0 \\
0 & -a/2 & 0 & -a/2 & 0 & a/2 & 0 & a/2 \\
0 & -a/6 & 0 & -a/3 & 0 & a/6 & 0 & a/3 \\
a^2/6b & 0 & a^2/3b & -a/2 & -a^2/6b & a/2 & -a^2/3b & 0 \\
-a/2 & -b/2 & -a/2 & b/2 & a/2 & -b/2 & a/2 & b/2
\end{bmatrix}$$

(vi) Matrix. $[T] = \phi\, [R]^T [L]\, ds.$